Detection of signals linked to climate change, land-cover change and climate oscillators in Tropical Montane Cloud Forests

Sietse O. Los[a], F. Alayne Street-Perrott[a], Neil J. Loader[a], Cynthia A. Froyd[b]

[a]*Department of Geography, Swansea University, Singleton Park, Swansea SA2 8PP, United Kingdom*
[b]*Department of Biosciences, Swansea University, Singleton Park, Swansea SA2 8PP, United Kingdom*

Abstract

Tropical Montane Cloud Forests (TMCFs) form biodiverse communities that are characterized by frequent occurrence of low-level clouds from which they capture a substantial proportion of their precipitation — here referred to as occult precipitation. TMCFs provide important ecosystem services, in particular the supply of water to their wider surroundings. Throughout the tropics (here 23.5° S to 23.5° N), they are under pressure from deforestation and poor land management which leads to loss of both forest area and species diversity, and reduces their capture of occult precipitation. Climate change may also reduce occult precipitation in TMCFs since the cloud base may lift in response to higher temperatures — the 'lifting cloud-base hypothesis'. These threats to TMCFs are well understood, but their quantitative

assessment is hampered by 1) uncertainty in the location and spatial extent of TMCFs and 2) limited availability of representative meteorological data. We use a Random Forest Classifier — informed by topographic data, MODIS vegetation data, TRMM precipitation data and ERA5-Land and MERRA-2 reanalysis products — to estimate the spatial distribution and extent of TMCFs (2.1×10^6 km^2 $\pm$ 0.5×10^6 km^2). We analyze temporal changes in climate, tree-cover and greenness of TMCFs over the past two to four decades to detect 1) multi-decadal trends, and 2) associations with the El Niño Southern Oscillation (ENSO) and Indian Ocean Dipole (IOD). Evidence for the 'lifting cloud-base hypothesis' in reanalysis products was inconsistent across the tropics; a lifting of the cloud base during the past four decades occurred for about 20 % of TMCFs, predominantly in the Americas and a few locations in Africa, while in Asia a downward movement of the cloud base was found. However, these results in part depend on the bias correction applied to the reanalyses. Changes in TMCF tree cover and greenness varied by continent; in Africa in ~50% of TMCFs tree cover declined, whereas TMCFs in the Americas and in Asia exhibited a net increase in tree cover, despite a reduction in tree cover in ~20% of TMCFs. An important limitation of the tree-cover data is that they do not distinguish between natural tree cover

and agro-forestry. ENSO signals were more strongly present in precipitation in American and Asian TMCFs, whereas IOD signals were stronger in TMCF temperature and dewpoint temperature across the tropics. ENSO and IOD signals were approximately equally important for precipitation in African TMCFs and in cloud-base height across the tropics. An arbitrary warming of 1 °C and a 100 m lifting of the cloud base, in accordance with the 'lifting cloud hypothesis', imposed on the Random Forest classifier showed a decline in the extent of TMCFs in the Americas and Africa, but an increase in Asia — mostly at the expense of evergreen broadleaf forests. The greater vulnerability of TMCFs in Africa may be linked to their more isolated and scattered distribution across the continent and drier conditions compared to a more continuous distribution and wetter conditions in the Americas and Asia.

Keywords: Climate Change — Tropical Montane Cloud Forests — Cloud-base height — ENSO — IOD — Reanalysis — TRMM — MODIS

1. Introduction

Formulating a precise definition of tropical montane cloud forests (TMCFs) is not straightforward (Hamilton et al., 1995). TMCFs tend to be tropical forests, for the main part located above 500 m a.s.l., that experience persistent low-level cloud cover for at least part of the year; the moisture captured by the vegetation canopy from these low-level clouds, referred to as occult precipitation, forms a large proportion of total precipitation. TMCFs are unique ecosystems that host a range of highly specialised organisms, often adapted to foggy conditions, such as epiphytes, bryophytes, amphibians, and insects (Pounds et al., 1999; Still et al., 1999; Foster, 2001; Karmalkar et al., 2008; Hemp, 2009; Bruijnzeel et al., 2010, 2011; Diaz et al., 2014; Lister and Garcia, 2018). Trees in TMCFs tend to have reduced height and greater stem density and their form, in particular at higher elevations, is often stunted or gnarled (Grubb and Whitmore, 1966; Cavelier, 1996; Bruijnzeel et al., 2010). TMCFs provide important ecosystems services; a stable supply of fresh water to their surroundings is particularly important (Asquith et al., 2008; Martínez et al., 2009).

TMCFs are adversely affected by human actions such as clear-cutting and use of forests as a source for firewood, food, medicines and fodder for livestock (Martínez et al., 2009; Cuní-Sanchez et al., 2018); the loss in forest cover is estimated larger for 'cloud affected' montane forests (55–60 %) than for other tropical forests (ca 47 %) (Doumenge et al., 1995; FAO, 1995; Mulligan and Burke, 2005). A reduction in the density of the forest canopy, associated with human activities, has an additional effect in that it reduces the ability of forests to capture water from clouds. Global warming poses a threat as well because of the potential for the cloud base to lift gradually as temperatures increase, thereby putting an important source of moisture out of reach of the canopy; this mechanism is known as the 'lifting cloud-base hypothesis' (Pounds et al., 1999; Bradley et al., 2004; Williams et al., 2007; Fu et al., 2011; Ohmura, 2012; O'Gorman and Singh, 2013; Oliveira et al., 2014; Helmer et al., 2019). On tall mountains, not disturbed by humans, there is sufficient room for TMCFs to move to higher altitudes to accommodate upward movements of the cloud base, but on mountains of moderate height or on mountains where the treeline is suppressed by humans (Bush et al., 2008; Di Pasquale et al., 2008; Sylvester et al., 2017), a higher cloud base could lead to "mountain-top extinctions" (Pounds et al., 1999; Still et al., 1999; Bruijnzeel et al., 2011).

The mechanisms that adversely affect TMCFs are well understood but quantifying their effects is hampered by two factors: the first is that the spatial extent and locations of TMCFs are not well known — current estimates vary by an order of magnitude between 0.22×10^6 km^2 and 2.2×10^6 km^2 (Mulligan and Burke, 2005; Scatena et al., 2010; Bruijnzeel et al., 2011);

and the second is that relatively few representative long-term meteorological records exist for the tropics. Jarvis and Mulligan (2011) find that meteorological stations measuring rainfall have an average distance to a cloud forest of 21 km; those measuring 2 m surface temperature 38 km; and those measuring the daily temperature range 53 km. Hence, in many cases these stations do not represent meteorological conditions in the TMCFs; moreover, large gaps frequently occur in these records.

The present study has two aims. The first is to obtain an estimate of the spatial extent and distribution of TMCFs. To this effect a random forest classifier is informed by a wide range of data sources: topographic data, normalized difference vegetation index data from the Moderate Resolution Imaging Spectroradiometer (MODIS), precipitation data from the Tropical Rainfall Measuring Mission (TRMM), and temperature and dew-point temperature products from the European Centre for Medium-Range Weather Forecasts Reanalysis (ERA5-Land) and the NASA Modern-Era Retrospective analysis for Research and Applications Version 2 (MERRA-2). Because of the unique meteorological conditions found in TMCFs, it is thought that climate information contained in reanalysis products will make an important contribution to the estimation of their extent. The second aim of the present study is to use the spatial distribution of the TMCF land-cover class to answer the following questions linked to changes in the climate and environment of TMCFS over the past two to four decades: 1) are temperatures increasing? 2) Is there evidence that the cloud base has lifted during the recent past as a result of global warming? 3) Is precipitation (rainfall) affected? 4) Is there a noticeable decrease in vegetation greenness? 5) Is tree-cover decreasing? 6) How do these changes (if any) compare to those found in tropical land-cover classes in particular evergreen broadleaf forests? 7) Do climate oscillators (the El Niño Southern Oscillation and Indian Ocean Dipole) have an effect on TMCFs? And 8) can we expect the spatial extent of TMCFs to change in response to a lifting of the cloud base as a result of global warming?

We acknowledge that the adopted approach has limitations, most of which are related to the relatively low spatial resolution of the data products (all scaled to $0.1° \times 0.1°$), but nevertheless it is able to provide an assessment of TMCF extent and to identify where the most severe pressures on TMCFs have occurred at continental scales during the past two to four decades.

2. Data sources and adjustments

The data sets used in the present study have different spatial resolutions. Raster data with low resolutions ($\leq 0.25^\circ \times 0.25^\circ$) are scaled to the $0.1^\circ \times 0.1^\circ$ spatial resolution of the ERA5-Land products using bi-linear interpolation (Hijmans, 2019); higher resolution data are averaged. The station data (Smith et al., 2011) and TMCF location data (Aldrich et al., 1997) are assigned to the corresponding $0.1^\circ \times 0.1^\circ$ cell.

2.1. ERA5-Land and MERRA-2 2 m temperature and dew-point temperature

The ECMWF Reanalysis 5 ERA5-Land version 1.0 (Copernicus Climate Change Service (C3S), 2019) is a recent release by the ECMWF that replaces the ERA-Interim. We use the ERA5-Land monthly 2 m temperature and dew-point temperature from 1981 until 2019 at $0.1^\circ \times 0.1^\circ$ spatial resolution (Copernicus Climate Change Service (C3S), 2017, 2019).

Cloud-base height, Z_C (m), is approximated from ERA5-Land 2 m temperature and dew-point temperature using Espy's equation. The approximation has an error smaller than 2 % for relative humidity values above 50 % and temperatures between 0 °C and 30 °C (Lawrence, 2005):

$$Z_C = 125(T_{2m} - T_{d,2m}), \tag{1}$$

with T_{2m} being the 2 m air temperature and $T_{d,2m}$ the dew-point temperature (both in either K or °C).

MERRA-2 (Gelaro et al., 2017) was developed by the NASA Global Modeling and Assimilation Office (GMAO) to meet two primary objectives: 1. to assimilate data from NASA's Earth Observation System (EOS) and to demonstrate its usefulness for climate studies and 2. to improve the representation of the atmospheric hydrological cycle in reanalysis models compared to previous ones. MERRA-2 has a resolution of 0.625 ° longitude by 0.5° latitude and covers a period from January 1980 until the present. We use monthly MERRA-2 2 m temperature, T_{2m}, dew-point temperature, $T_{d,2m}$, and cloud-base height, Z_C, from 1980 until 2019.

2.2. Meteorological observations from station data

We use 2 m surface-air temperature and dew-point temperature contained in the National Oceanic and Atmospheric Administration (NOAA) National Climatic Data Center (NCDC) Integrated Surface Data set (ISD; Smith et al. (2011)) to check the reanalyses for bias. Annual averages are calculated from daily averages when there are fewer than 20 days of data missing per year. Station data are assigned to the corresponding $0.1° \times 0.1°$ cell. The temporal coverage of meteorological data varies from year to year; the minimum number of cells with at least one station operating for more than 345 days per year during 1980–2019 is around 670, the average around 960, and the maximum close to 1500. The reduced ISD data set used in the present study is a subset of both the World Meteorological Organization (WMO) station data used by ERA5-Land and of the Global Historical Climate Network (GHCN) data used by MERRA-2.

2.3. Bias correction of ERA5-Land and MERRA-2 T_{2m} and $T_{d,2m}$

Both the ERA5-Land and MERRA-2 reanalyses show good agreement with observations — the coefficients of correlation with station data are high for both and the biases are low. The biases are smaller and less negative for MERRA-2 than for ERA5-Land $T_{2\mathrm{m}}$ and $T_{d,2\mathrm{m}}$ but correlations are lower as well (Table 1). In both reanalyses, $T_{2\mathrm{m}}$ and $T_{d,2\mathrm{m}}$ show a drift in bias over time relative to the ISD observations. Similar, but smaller drifts occur as a function of longitude, latitude and altitude; an example is shown in Fig. 1 for ERA5 $T_{d,2\mathrm{m}}$. Trends in these drifts are estimated using:

$$\begin{aligned}\Delta_{\mathrm{drift}} = \beta_0 + \beta_1\cos(x) + \beta_2\sin(x) + \beta_3\cos(y) + \\ \beta_4\sin(y) + \beta_5 z + \beta_6\cos(z) + \beta_7 sin(z) + \\ \beta_8 h + \beta_9\cos(x)\sin(x)\cdots + \beta_{36} sin(z)h\end{aligned} \quad (2)$$

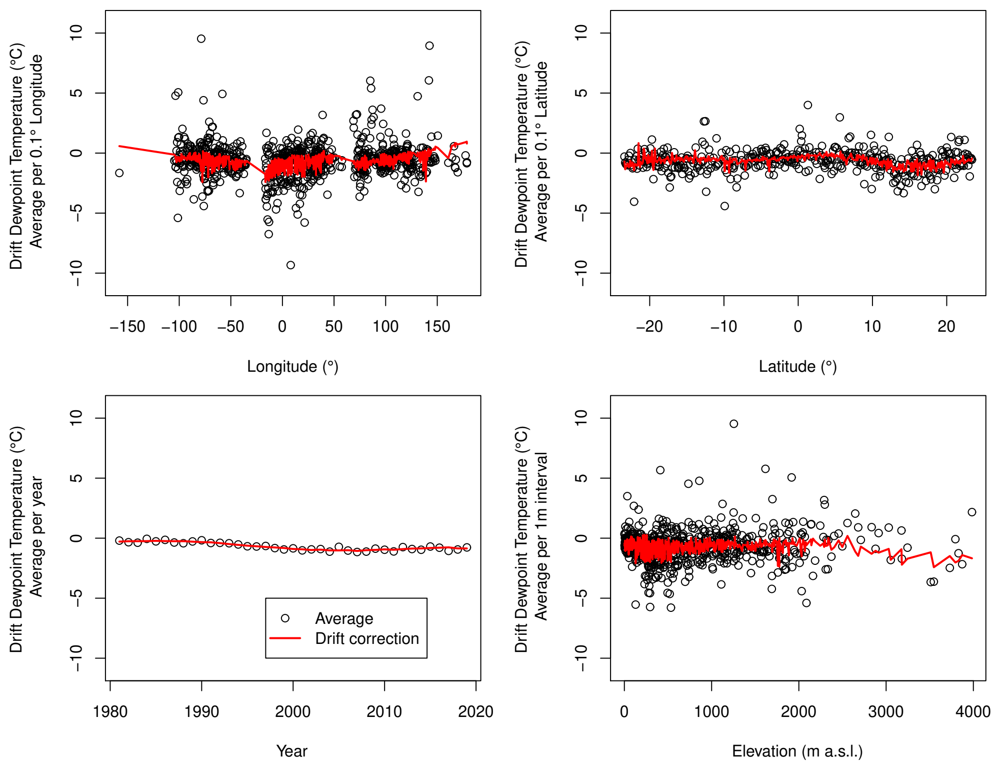

Figure 1: Average drift in dew-point temperature (difference between ERA5-Land and observations) shown as a function of longitude, latitude, time and elevation. The red line shows the drift correction obtained with eq. 2.

with Δ_{drift} being the difference of either ERA5-Land or MERRA-2 mean annual $T_{2\text{m}}$ or $T_{d,2\text{m}}$ from observations, x the latitude converted to radians ($-180°...180°$ is one wavelength), y the same as x but for longitudes from 23.5° S to 23.5° N, z the year (1981..2019 for ERA5-Land, 1980..2019 for MERRA-2; for the trigonometric functions the year is converted to radians

Table 1: Comparison of ERA5-Land and MERRA-2 2 m surface-air temperature (T_{2m}), 2 m dew-point temperature ($T_{d,2m}$) and cloud-base height (Z_C) with meteorological station data for the entire tropics before and after bias correction (eq. 2). The bias correction increases the secular trend in dew-point temperature and reduces the secular trend in cloud-base height.

	ERA5-Land	correction	MERRA-2	correction
r ISD T_{2m}	0.80	0.81	0.59	0.66
bias ISD T_{2m} (K)	-1.1	0	-0.6	0
r ISD $T_{d,2m}$	0.89	0.89	0.79	0.81
bias ISD $T_{d,2m}$ (K)	-0.7	0	-0.2	0
r ISD Z_C	0.88	0.88	0.80	0.83
bias ISD Z_C (m)	-56	-0.8	-42	-0.7
trend T_{2m} (K y^{-1})	0.023	0.029	0.023	0.028
trend $T_{d,2m}$ (K y^{-1})	0.004	0.026	0.011	0.022
trend Z_C (m y^{-1})	2.4	0.37	1.6	0.7

with the length of one wave matching the entire time period) and h the elevation. Trigonometric functions are used rather than second or higher order polynomials to avoid extrapolation errors when applying the bias correction. The bias correction improves the correspondence with the station observations; it also reduces the temporal trend in cloud-base height for the tropics and trends in ERA5-Land and MERRA-2 cloud base are more similar after the drift correction is applied (Table 1). The decrease in coverage over time by meteorological stations appears to have a negligible effect on the bias correction.

2.4. TRMM 3B43 precipitation

The Tropical Rainfall Measuring Mission (TRMM) was designed to fill important gaps in the previous land and ocean surface precipitation record between latitudes of 40° S and 40° N (Simpson et al., 1988). The 3B43 record starts in 1998 and has $0.25° \times 0.25°$ spatial resolution, a monthly time step and covers latitudes between 50° S and 50° N. This product combines data from the TRMM satellite, the Global Precipitation Climatology Project (GPCP) ground station network, and the Aqua, Terra, Defence Meteorological Satellite Program and NOAA satellites (Huffman et al., 2007, 2010).

2.5. Satellite vegetation data

We obtained MODIS Terra Normalized Difference Vegetation Index (NDVI) data version 6 (Huete et al., 2002) projected on a climate modelling grid at $0.05° \times 0.05°$ resolution from the United States Geological Survey (USGS).

We applied Fourier series (annual and 6 month harmonics) to these data to fill in missing values and adjust outliers caused by interference from clouds and aerosols; the procedure is similar to the method developed by Sellers et al. (1996) and Los et al. (2000) — Fourier series are used to adjust per cell the entire time series using a moving window of 12 months that is shifted 6 months at a time. For each 12-month window, Fourier series are fitted using weighted regression to identify and replace outliers and missing data. For the first and last window of the time series the first and last 9 monthly values are used, for the other windows the central 6 values. After the Fourier adjustment is applied, the spatial resolution of the data is reduced to $0.1° \times 0.1°$ by calculating the mean of a window of 2×2 pixels. The standard deviation of this window is calculated as well to retain information about spatial variability. A monthly climatology consisting of the average seasonal cycle is calculated per cell from both the average and standard deviation time series. The minimum, average and maximum values of these climatologies are used as independent variables in the land-cover classification (Section 3.1).

Annual MODIS International Geosphere Biosphere Programme (IGBP) land-cover data (Friedl et al., 2010; Sulla-Menashe et al., 2019) are obtained from the USGS for the years 2001 until 2018. We use the percentage cover

Table 2: Rules applied to International Geosphere-Biosphere Programme (IGBP) tropical land-cover classes to aggregate them into broader units. The following IGBP classes are not included because of very low coverage in the tropics: Deciduous Needle-leaf Forests (IGBP class 3), Permanent Wetlands (11), Urban and Built-up (13), and Snow and Ice (16).

Class (present study)	Abbreviation		IGBP class
1. Tropical Montane Cloud Forest	TMCF		-
2. Evergreen Broadleaf Forest	EBL	2.	Evergreen Broadleaf Forest
3. Deciduous Broadleaf Forest	DBL	4.	Deciduous Broadleaf Forest
		5.	Mixed Forest
		8.	Woody Savanna
4. Savanna	SAV	9.	Savanna
5. Shrub land	Shrub	6.	Closed shrub lands
		7.	Open shrub land
6. Grassland	Grass	10.	Grasslands
7. Cropland	Crop	12.	Croplands
		14.	Crop + natural vegetation mosaic
8. Barren	Barren	16.	Barren

for each of the IGBP land-cover classes averaged over this period. The land-cover classes are grouped into 7 larger units according to the rules set out in Table 2.

The 'Making Earth System Data Records for Use in Research Environments' (MEaSUREs) Vegetation Continuous Fields version 001 data (Song et al., 2018) are obtained from the USGS. This data set provides annual updates of tree-cover fraction at $0.05^\circ \times 0.05^\circ$ resolution. Tree-cover fraction in the MEaSUREs data set is estimated from cross-calibrated Advanced Very High Resolution Radiometer (AVHRR), MODIS and Landsat data; the data set is sufficiently accurate for change detection. A limitation is that the MEaSUREs tree-cover data do not distinguish between natural trees and agroforestry (Song et al., 2018).

2.6. Topography

The Global Multi-resolution Terrain Elevation Data 2010 at 30 arc-seconds resolution (GMTED2010, Danielson and Gesch (2011)) has improved vertical accuracy compared to the GTOPO30 data set that it replaces (the root mean square errors (RMSEs) are 25–42 m and 66 m, respectively). The improvement is due to, amongst other things, the incorporation of data from the Shuttle Radar Topography Mission (SRTM) and the Ice, Cloud, and Land

Elevation Satellite (ICESat).

2.7. Distance to the coast

Distance to the coast at $0.01^\circ \times 0.01^\circ$ resolution was obtained from the OceanColor project which used the Generic Mapping Tools (GMT) software (Wessel and Luis, 2017) to generate this data set (Stumpf and Kuring, pers. comm.).

2.8. Country data

We use the Natural Earth data (https://www.naturalearthdata.com/) to identify boundaries used to calculate country statistics shown in Tables S2 and S3. The land-sea mask in this data set differs slightly from that used in the other data sets.

2.9. Locations of cloud forests

The cloud-forest location data base was compiled by Aldrich et al. (1997) and is held at the World Conservation Monitoring Centre (WCMC). This data base was obtained from local experts and is considered the best available information on the location and status of TMCFs (Aldrich et al., 1997). The data set contains 525 TMCF locations, but does not provide information about their spatial extent, dominant species or degree of disturbance.

TMCFs within International Union for Conservation of Nature (IUCN) protected zones (Americas (4 %), Africa 39 % and south-east Asia 50 %) tend to be larger and more continuous, but outside of these they tend to be more patchy. Information about the effects of humans on TMCFs, which become increasingly important over time (Power et al., 2008; Bush et al., 2011; Sublette Mosblech et al., 2012; Sylvester et al., 2017; Marchant et al., 2018), is not available. Further limitations of the data base are that some cloud-dependent ecosystems such as the uplands of the Galápagos Islands are naturally shrub or grass-dominated; other locations are situated below an altitude of 500 m, the generally accepted lower boundary of TMCFs (Jarvis and Mulligan, 2011). The low-altitude locations are retained in the current analysis. The Aldrich et al. (1997) data are the basis of several subsequent estimates of the spatial extent of TMCFs (Bubb et al., 2004; Mulligan, 2010; Jarvis and Mulligan, 2011). For example Jarvis and Mulligan (2011) used MODIS land-cover data and combined these with topographic measurements and estimates of immersion of the canopy by fog and low-level clouds and refer to these areas as 'significantly cloud-affected forests'.

The number of TMCF locations is reduced to 466 when the data are scaled to $0.1^\circ \times 0.1^\circ$ because multiple locations map onto the same cell. A further 6 data points are lost when the locations are used in the Random Forest Classifier (section 3.1) because of missing data in one or more of the independent variables.

3. Analysis and Results

3.1. RF-based estimation of TMCF spatial extent

We estimate the spatial extent of TMCFs using a Random Forest Classifier (Breiman, 2001; Liaw and Wiener, 2002). Random Forest Classifiers average the outcome of multiple decision trees to calculate class probability. The algorithm uses cross-validation; a proportion of the training data is set aside to test the accuracy of the classification. Random Forest Classification is less sensitive to overfitting than most other classification method. We aim to classify TMCFs and the aggregated MODIS IGBP classes to obtain a uniform classification consisting of the 8 classes in Table 2. The training sites are obtained from two sources: the 460 centre locations of TMCFs compiled by Aldrich et al. (1997) scaled to $0.1^\circ \times 0.1^\circ$ and randomly selected sites from the aggregated MODIS IGBP land-cover classification (Friedl et al. (2010); Sulla-Menashe et al. (2019); Table 2). From each of the aggregated MODIS classes, 999 sites are selected from pixels where cover for a particular class is

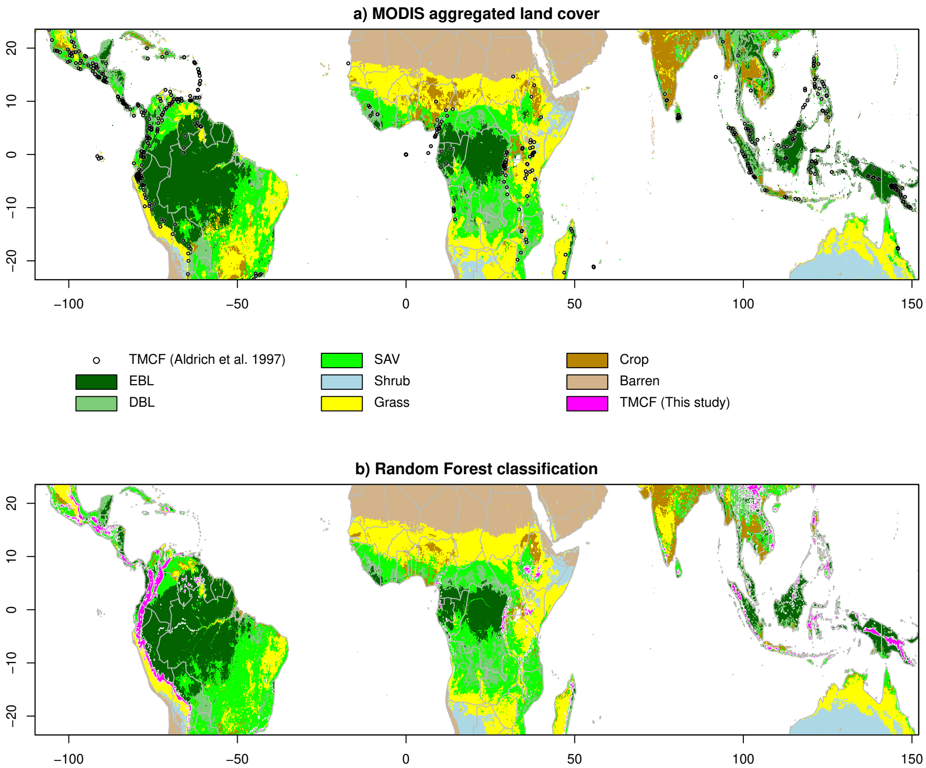

Figure 2: a) MODIS IGBP land-cover classification aggregated into 7 classes (Table 2). The locations of Tropical Montane Cloud Forests from Aldrich et al. (1997) are indicated by circles. b) Distribution of land-cover classes (including TMCFs) obtained using a Random Forest Classifier (Liaw and Wiener, 2002; Breiman, 2001); an accuracy assessment is provided in Table 3. The spatial distribution of TMCFs (probability and dominant class) is provided in the Supplement in GeoTIFF format).

larger than 75 %. MODIS training sites that overlap with the TMCF training sites are identified as TMCFs and their MODIS class is ignored.

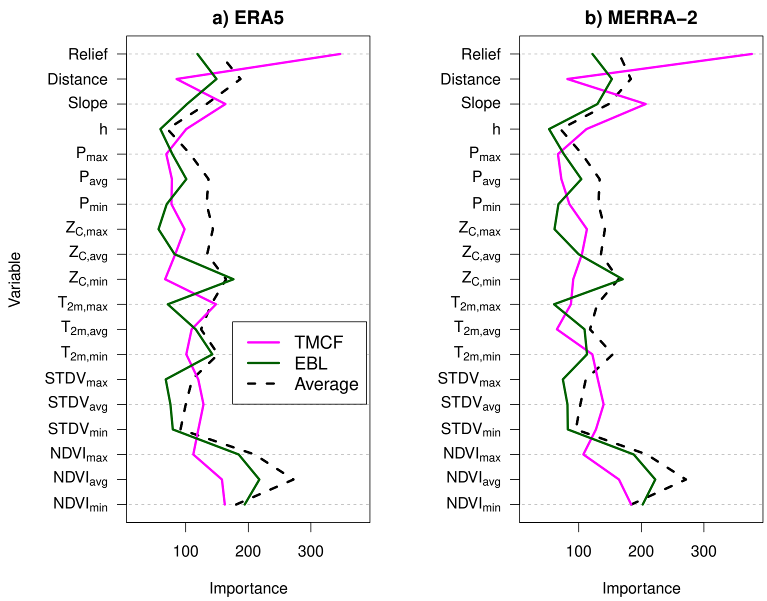

Figure 3: Importance of variables used to classify TMCFs (continuous magenta line) compared to the same for broadleaf evergreen forests (continuous dark green line) and the average of all classes (dashed black line). Importance is the effect that permutation of a particular variable has on the Random Forest classification results (Liaw and Wiener, 2002; Breiman, 2001). Variable h indicates the altitude, P the TRMM precipitation amount, Z_C the cloud-base height (eq. 1), $T_{2,m}$ the 2 m surface air temperature and STDV the spatial standard deviation in NDVI calculated from windows of 2×2 pixels (Section 2.5).

Both static and time-variant independent variables were used for the land-cover classification (Section 2). Static independent variables are altitude, relief (the difference between minimum and maximum altitude for each $0.1^\circ \times 0.1^\circ$ cell), distance from the coast, and $\Delta h/\Delta d$, the change in elevation as a function of distance from the coast (Section 2). This variable is the slope coefficient determined from linear regression on data of each $0.1^\circ \times 0.1^\circ$ cell with Δh the dependent variable and Δd the independent variable. Time-variant independent data include, for each $0.1^\circ \times 0.1^\circ$ cell, the minimum, average and maximum of the NDVI climatology calculated from 2001-2019 data. The same three statistics were used for the climatology of the spatial standard deviation in NDVI (STDV). A higher standard deviation is likely associated with disturbance and greater human influence on land cover. Other independent data used in the classifier are the minimum, average and maximum seasonal values of 2 m temperature (T_{2m}), cloud base height (Z_C, eq. 1), and precipitation (P). The use of minimum, average and maximum provides information about the shape of the seasonal cycle; e.g. the warm season is longer if the average temperature is closer to the maximum and shorter if it is closer to the minimum.

The number of decision trees for the Random Forest Classifier is set to 20,000; the Random Forest classification is then carried out separately using either the ERA5-Land or MERRA- T_{2m} and $T_{d,2m}$ products at $0.1^\circ \times 0.1^\circ$ resolution. The Random Forest Classifier adds outcomes of individual decision trees to estimate the overall probability for a particular class. The Random Forest Classifier also estimates out-of-bag (OOB) errors (Breiman, 2001) for each of the classes as well as a confusion matrix (Table 3). Similar accuracy is achieved for both re-analysis products. The largest confusion between classification results occurs between TMCFs and evergreen broadleaf forests (for the ERA5-Land classification 58 predictions of EBL are made where the actual class is TMCF, and 36 predictions of TMCFs where the actual class is EBL, Table 3; the results for MERRA-2 are similar; see Table S1). Confusion of TMCFs with other, drier classes occurs as well. An explanation for this is that some TMCFs, mostly located in Africa, are small in size ($< 0.1^\circ \times 0.1^\circ$ cell) and are surrounded by much drier environments; examples are TMCFs located on the summits of dormant volcanoes in Kenya that are surrounded by much drier shrub lands and deserts (Bussmann, 2002; Cuní-Sanchez et al., 2018). In some cases, the Aldrich et al. (1997) data refer to the remnants of TMCFs that survived extensive clearing of trees over the past centuries (Aldrich et al., 1997; Marchant et al., 2018) and the classifier may indicate a TMCF where shrub land remains and in other cases the Aldrich et al. (1997) data refer to cloud-dependent forests where non-tree species are dominant. As a result, the estimated TMCF distribution includes a small proportion of cells with very low or no tree cover ($< 10\,\%$). This proportion of cells is smaller for the ERA5-Land based classification ($3\,\%$) than for the MERRA-2 based classification (5 %).

The probability values representing the likelihood that a particular class occurs in a cell, correlate highly with MODIS cover fractions (Table 3) indicating compatibility with the MODIS land-cover classification despite the relatively low spatial resolution of the independent variables.

Importance of a variable for the classification is estimated by calculating the effect of permuting the variable on the outcome of the classification. By this definition, the most significant variables for the classification of TMCFs are relief and slope and NDVI (min and max) and spatial variability in NDVI (STDV avg, min, max; Fig. 3). Of the variables associated with cloud-base height, the maximum ($Z_{C,\max}$) is the most important for both the ERA5-Land and MERRA-2 based classifications. The precipitation variables are among the least important for the classification of TMCFs.

3.1.1. Effects of T_{2m} and Z_C on classification

The effect of T_{2m} and Z_C fields on the performance of the classification is further assessed by comparing the classification results obtained with the ERA5-Land and MERRA-2 products with one that uses neither (no reanalysis – NR; Table 4). The overall error for the NR classification is higher (η = 7.2 %) than those for the reanalysis-based classifications (η = 5.7 %), and the ERA5-Land and MERRA-2-based classifications show better agreement with each other ($\eta = 5.4\,\%$) than with the NR classification ($\eta = 8.0\,\%$ or $7.9\,\%$). However, for TMCFs the disagreement between the reanalysis-based classifications is larger (14.2 %) than the disagreement of either with the NR classification (13.9 % and 12.6 %). Disagreement for all other classes was smallest between the reanalysis-based classifications; disagreement between the NR classification and the reanalysis based classifications is particularly large for deciduous broadleaf forests (17.9 % and 16.6 %), shrubs (11.4 % and 11.1 %), and crop lands (22.2 % and 24.1 %). These classes cover smaller areas and show a relatively large degree of confusion with each other. A relatively low agreement is also indicated by the lower correlations between the class probability calculated by the Random Forest Classifier and the MODIS fractional cover in Table 3.

3.1.2. Evaluation and summary of classification results

The spatial extent of TMCFs and of seven aggregated MODIS-IGBP land-cover classes was estimated with a Random Forest Classifier. The largest uncertainty was in the estimation of TMCFs (24 %); the range in uncertainty for the other classes was between 0 % (Barren land cover) and 7 % (Crop land). The disagreement between different approaches to estimate the spatial extent of TMCFs (ERA5-Land, MERRA-2, no reanalysis) was smaller (12 % – 14 %) than the uncertainty indicated by the RF classification. TMCFs were most easily confused with broadleaf evergreen forests (13 %; Table 3). The relatively large uncertainty in the classification of TMCFs is not surprising since the training data (Aldrich et al., 1997) have a fairly large degree of uncertainty as well (Jarvis and Mulligan, 2011; Bruijnzeel et al., 2011).

TMCF area estimates for 25 countries are compared to the ‘cloud affected’ tropical montane forests from Mulligan and Burke (2005). The agreement is good for the Americas and Asia (Fig. S1; note that the results for Brazil are not comparable since Mulligan and Burke (2005) compiled statistics for all of Brazil and in the present study only the tropical part of Brazil is considered). For several African countries, in particular for the Democratic Republic of the Congo, the estimates by Mulligan and Burke (2005) are much higher.

Orography (relief and slope) was the most important factor for the identification of TMCFs, most likely because the forced uplift of ocean air increases relative humidity leading to more frequent occurrence of supersaturated conditions and low-level clouds. Measures of NDVI seasonality and spatial variability in NDVI were also important for the identification of TMCFs as were some of the reanalysis temperature statistics and maximum cloud-base height (Fig. 3).

The largest extent of TMCFs is found in the Americas (~$1.0 \times 10^6\,\mathrm{km}^2$), followed by Asia (~$0.8 \times 10^6\,\mathrm{km}^2$), and the smallest extent in Africa (~$0.3 \times 10^6\,\mathrm{km}^2$; Tables S2 and S3). Statistics collated for countries with the largest TMCF cover indicate differences between continents. There are indications that TMCFs in Africa are either smaller or more patchy than in other continents, since (1) the probability in cells where TMCFs are the dominant class is lowest in Africa (0.54 (ERA5-Land) or 0.55 (MERRA-2) versus 0.69 or 0.68 in the Americas and 0.61 or 0.57 in Asia; Tables S2 and S3), (2) the vegetation cover for African TMCFs is lower (lower mean NDVI, Tables S2 and S3), (3) is more spatially variable (higher spatial standard deviation in NDVI, Tables S2 and S3) and (4) contains a higher percentage of crop land (Tables S2 and S3). African TMCFs are drier as well; the amount of TRMM precipitation is lower, the cloud-base height higher and the distance to the ocean larger (Tables S2 and S3). TMCFs in Asia tend to be warmer (~24°C versus ~20°C both in the Americas and in Africa) and are found in lower altitudes than on other continents (994 m a.s.l. (ERA5-Land) or 812 m a.s.l. (MERRA-2) versus 1771 or 1695 m a.s.l. in the Americas and

1642 or 1656 m a.s.l in Africa) and the atmosphere tends to contain a higher amount of moisture (the average cloud-base height is lower in Asia (358 m (ERA5-Land) or 435 m (MERRA-2)) versus that in the Americas (418 m or 583 m) or Africa and (596 m or 696 m; Tables S2 and S3).

For the overall classification of 7 IGBP classes, NDVI measures (climatological minimum, average and maximum), distance to the coast and measures of cloud-base height and temperature were the most important (Fig. 3). Grasses and crops showed the biggest improvement in identification from incorporation of reanalysis temperature and cloud-base height followed by shrubs and deciduous broadleaf forests (Table 4).

3.2. Detection of trends and variability in temperature, cloud-base height, precipitation, NDVI and tree cover

Variability and trends in climatic and environmental variables in TMCFs, as identified by the Random Forest Classification (Section 3.1), are analyzed over the past two to four decades. Variables investigated are surface-air temperature, dew-point temperature, cloud-base height (1980/1981 – 2019), precipitation (1998 – 2019), NDVI (2000 – 2019) and tree cover (1982 – 2016; Section 2); for these variables the secular trends are calculated for the time span over which data are available (Tables 5, S4). Furthermore, associations

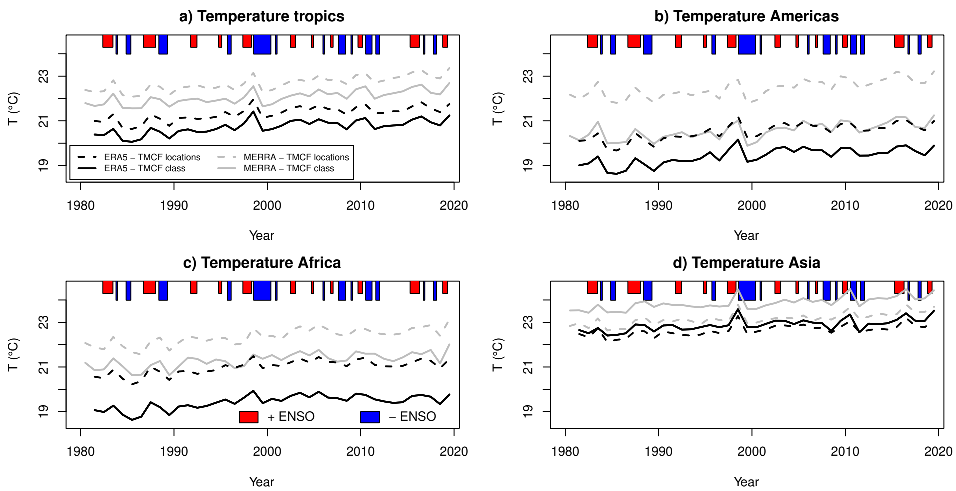

Figure 4: Temporal variations in MERRA-2 and ERA5 Land 2 m temperatures for TMCFs from 1981 (ERA5-Land) or 1980 (MERRA-2) until 2019. Continuous lines show averages for the TMCFs obtained from the Random Forest Classifier (Section 3.1); dashed lines show averages for the central locations of TMCFs in the Aldrich et al. (1997) data. The boxes indicate when the Oceanic Niño Index, the three month running average of the ERSST.v5 (Huang et al., 2017) for the Niño-3.4 region, is 0.7 °C above (red) or below (blue) average. a) Average land-surface temperatures for all TMCFs (sign test between occurrences of the Oceanic Niño Index (ONI) outside ±0.7°C and positive or negative anomaly in MERRA-2 or ERA5-Land temperature is significant ($p < 0.05$) for both; but r is not significant (NS) for either). b) Average for TMCFs in the Americas (South America, Central America and North America; sign test $p < 0.05$; r (ERA) NS; r (MERRA-2) = 0.44). c) Average for Africa (sign test $p < 0.05$; r NS). d) Average for Asia (sign test (ERA) NS; sign test (MERRA-2) $p < 0.05$; r NS).

are investigated with two important climate oscillators: the El Niño Southern Oscillation (ENSO) (Ropelewski and Halpert, 1987; Philander, 1989) and the Indian Ocean Dipole (IOD) (Saji and Yamagata, 2003); their associations are reported in the figure captions (Figs 4, 6, 8, 12 and 14). The spatial extent of correlations between environmental variables and ENSO or IOD are shown in Figs 5, 7, 10, S11, 13 and 15 as well as in the Supplement; a comparison of the relative strength of ENSO and IOD averaged for the tropics and each of the continental regions is also provided in the Supplement.

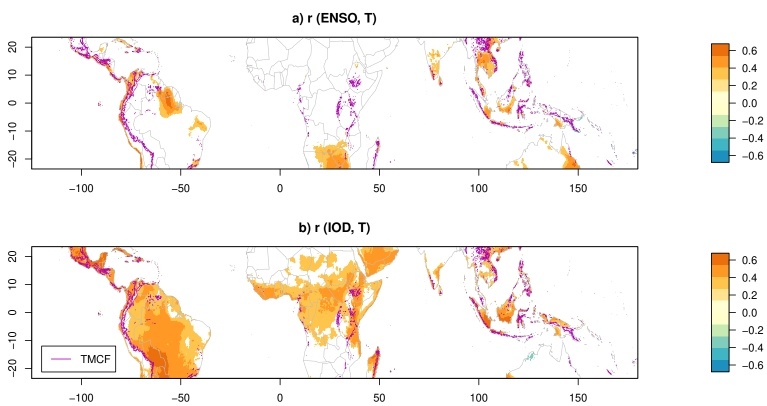

Figure 5: Correlation between mean ERA5-Land annual temperature (1981–2019) and a) ENSO (the average ERSSTv.5 of the Niño3.4 area); and b) IOD (Saji and Yamagata, 2003). Pixels where correlations are not significant are white. Boundaries of TMCFs are indicated by magenta lines. The IOD is significantly correlated with temperature for a larger number of cells than ENSO, in particular in the Americas and Africa (Fig. S3, S4).

3.2.1. Trends and variability in surface-air temperature

TMCF 2 m surface-air temperatures (bias adjusted; Section 2) are 1–2 °C lower for ERA5-Land than for MERRA-2, but their variability is similar ($0.85 < r < 0.93$, Fig. 4). The offset between ERA5-Land and MERRA-2 surface temperature is explained by a stronger association between altitude and temperature in ERA5-Land ($r = -0.85$) than in MERRA-2 ($r = -0.71$). The secular trends in temperature are between 0.01 and 0.02 °C per year and are highest in the Americas and in Africa. These trends are lower for ERA5 than for MERRA-2 land-surface temperatures and are smaller in TMCFs than in most other land-cover classes (Tables 5, S4). The link between ENSO and land-surface temperatures of TMCFs is complex. We use the Oceanic Niño Index (ONI) to define the occurrence and strength of ENSO events. The ONI is the three month running average of Extended Reconstructed Sea Surface Temperature (ERSST.v5) (Huang et al., 2017) anomalies in the Niño 3.4 region (5° S – 5° N and 120°-170° W). Here we use a threshold of ±0.7°C to identify a warm or cold ENSO event. In a similar way to ENSO, we use the Dipole Mode Index (DMI) to indicate the occurrence and strength of the IOD (Saji et al., 1999). DMI is the SST anomaly difference between the western (60° — 80° E, 10° S — 10° N) and eastern (90° — 110° E, 10°

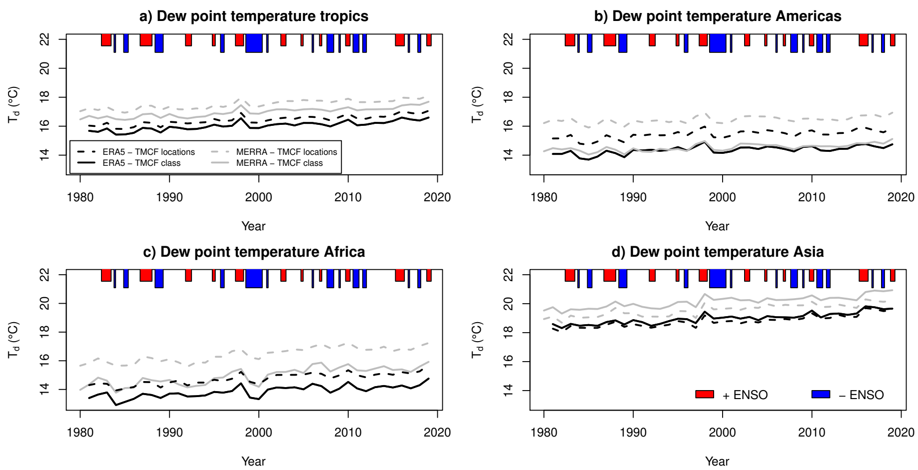

Figure 6: Same as Fig. 4 but for ERA5-Land and MERRA-2 dew-point temperature. a) (sign test between ONI and ERA5-Land or MERRA-2 dew-point temperature $p < 0.05$; r not significant (NS)). b) (sign test (ERA) $p < 0.05$; sign test (MERRA-2) NS; r (ERA5) $= 0.38$; r (MERRA-2) $= 0.33$). c) (sign test (ERA5) NS; sign test (MERRA-2) $p < 0.05$; r NS). d) (sign test (ERA5) $p < 0.05$; sign test (MERRA-2) NS; r NS).

S -–Equator) Indian Ocean. The correlation between DMI and ONI is low ($r = 0.3$ for 1981–2019 and $r = 0.05$ for 2001–2019), therefore simple, not partial, correlations with environmental variables are used in this section and the sections below.

The link between the above or below normal land-surface temperatures concurrent with a warm or cold ENSO event is significant for all time series with the exception of the ERA5-Land Asia time series. However, the correlation between the mean annual ONI and mean land-surface temperatures is only significant for MERRA-2 in the Americas. Hence, although it is possible to infer that land temperatures in TMCFs will increase or decrease during a warm or cold ENSO event, it not possible to infer the magnitude of that change.

Correlations between surface-air temperature and IOD are more extensive spatially than correlations with ENSO (Fig. 5); this is found across all regions. However, a large proportion of coastal areas in the Americas and Asia have significant correlations between surface-air temperature and ENSO, and hence ENSO is relatively important for temperatures in TMCFs.

3.2.2. Trends and variability in dew-point temperature

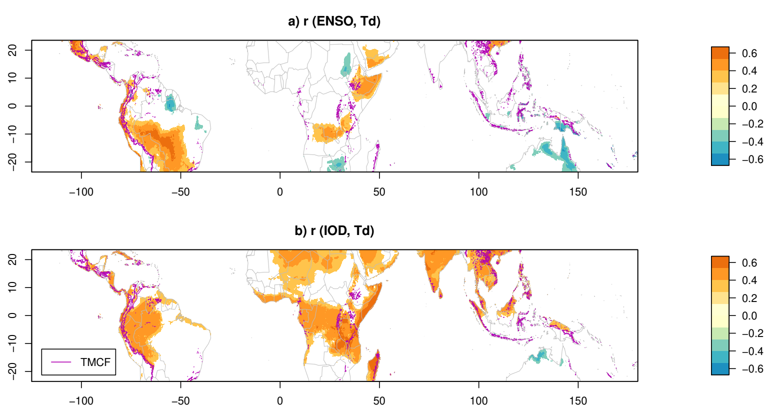

Figure 7: Same as Fig. 5 but for dewpoint temperature. The IOD is significantly correlated with dewpoint temperature for a larger number of cells than ENSO, in particular in Africa and Asia (Fig. S6, S7).

Year-to-year variability in the dew-point temperature time series is similar to that in the surface-air temperature time series (Fig. 6). ERA5-Land dew-point temperatures are lower than MERRA-2 dew-point temperatures, similar to surface-air temperatures. For both reanalyses, the secular trends in dew-point temperatures are higher than in surface-air temperatures (Table 5, S4). The influence of ENSO events is as follows (Fig. 6): warm and cold ENSO events lead to a corresponding increase or decrease in ERA5-Land dew-point temperature for the entire tropics, the Americas and Asia; and for MERRA-2 this relationship is significant for the entire tropics and Africa. The mean annual ONI has a significant positive correlation with mean annual dew-point temperatures in the Americas, but not in the other continents.

More areas have significant correlations of dewpoint temperature with the IOD than with ENSO; in particular, the absence of significant correlations with ENSO for most of Asia is remarkable. Similar to temperatures, correlations of dewpoint temperatures with ENSO and IOD are significant in many areas along coastal regions in the Americas where TMCFs are located.

3.2.3. Trends and variability in cloud-base height

The cloud-base height averaged over all TMCFs decreased over time, but this negative trend is not consistent; for example within continents areas with opposite trends are found. TMCFs in the Americas show an increase in

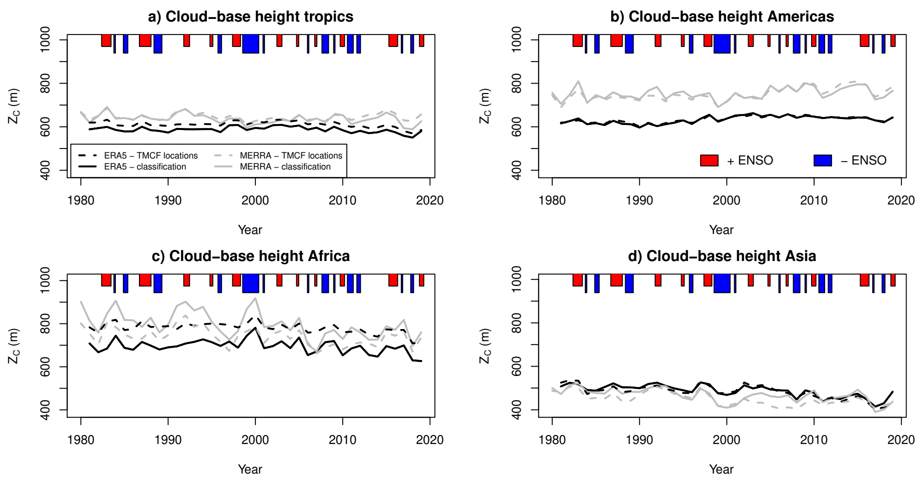

Figure 8: Same as Fig. 4 but for cloud-base height. a) (sign test between ONI and ERA5 cloud-base height $p < 0.05$; sign test (MERRA-2) NS; r (ERA) = 0.34; r MERRA) = 0.53). b) (sign test (ERA) NS; sign test (MERRA) $p < 0.05$; r (ERA)NS; r (MERRA) = 0.36). c) (sign test NS; r NS). d) (sign test NS; r (ERA) = 0.45; r (MERRA) = 0.55).

cloud-base height for large areas whereas for Asian TMCFs a decline in cloud-base height is predominant (Fig. 9, Tables 5, S4, S5). For the entire tropics, outside the TMCFs (Fig. 9), the cloud base lifted over most of the Americas and in large parts of Africa, and descended over most of Asia. Year-to-year variability in cloud-base height is smaller in ERA5-Land than in MERRA-2 (Fig. 9). The relationship between cloud-base height and ENSO events varies between continents: during a warm ENSO event areas on the American west coast and African east coast show a decline in cloud-base height, whereas throughout south-east Asia cloud-base height increases. Correlations be-

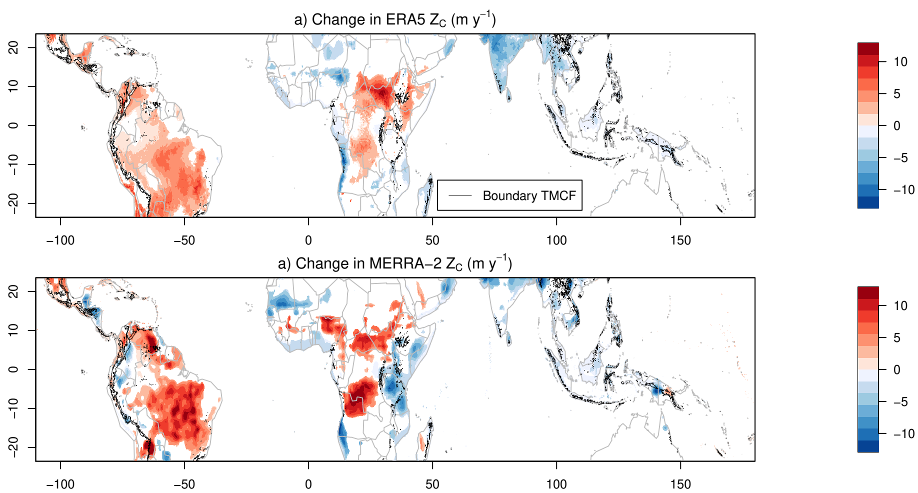

Figure 9: Secular trend in cloud-base height ($\mathrm{m}\,y^{-1}$) over the period of 1981–2019. America and Africa show a predominantly upward trend in cloud-base height in their interiors, whereas most of Asia shows a continued downward trend in cloud-base height.

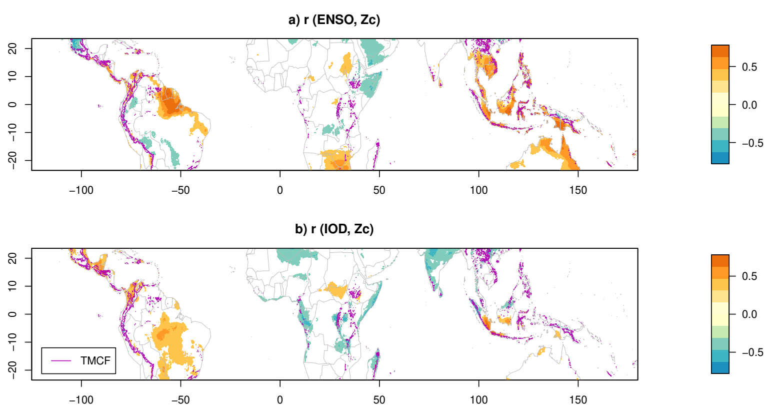

Figure 10: Same as Fig. 5 but for cloud-base height. The number of cells significantly correlated with either ENSO or the IOD is about the same for all continents (Fig. S9, S10).

tween ONI and cloud-base height are significant for the tropics; they tend to be negative for Africa and Asia and positive for the Americas (Fig. 9). The

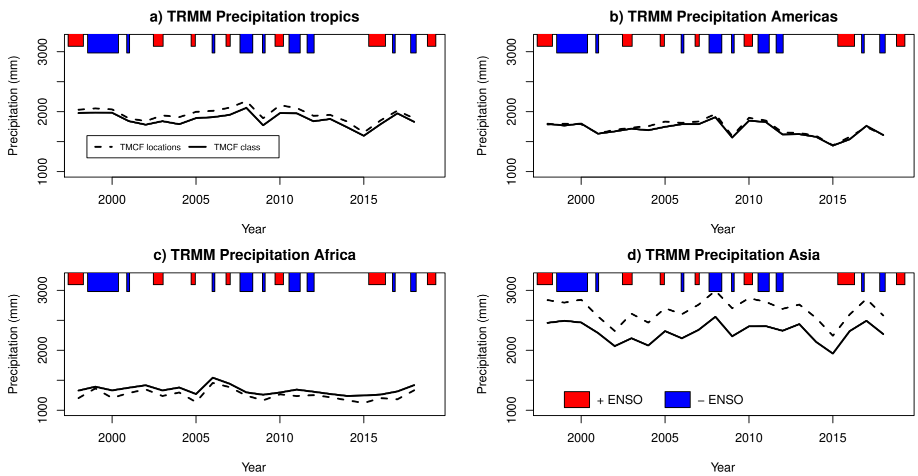

Figure 11: Same as Fig. 4 but for TRMM precipitation from 1998 until 2018 (no significant trend in any of the time series; none of the sign tests with the ONI are significant). a) ($r = -0.87$). b) $r = -0.73$. c) r NS d) $r = -0.85$.

number of TMCF cells throughout the tropics with significant correlations of cloud-base height and IOD is lower than for correlations with temperature or dewpoint temperature, but in Africa this number is relatively large. The number of significant correlations in all TMCFs of ENSO with cloud-base height, temperature and dewpoint temperature is similar (Fig. S9).

3.2.4. Trends and variability in precipitation

TRMM precipitation is lowest for the African TMCFs and highest for the Asian TMCFs. TMCF precipitation data averaged by continent do not show any secular trends. A significant negative correlation exists between the strength of the ENSO ONI signal and average TMCF precipitation for the tropics ($r = -0.82$), the Americas ($r = -0.5$) and Asia ($r = -0.77$). Other relationships between ENSO and precipitation are not significant; the lower number of ENSO events during the shorter length of the time series (compared to the reanalysis time series) is probably a contributing factor. The spatial distribution of correlations between precipitation and ENSO (Ropelewski and Halpert, 1987) or IOD (Saji and Yamagata, 2003) have been published elsewhere; however, they are included in the Supplement to provide figures that are consistent with the analysis of other variables (Fig. S11). The number of cells significantly (negatively) correlated with ENSO is much larger than the number of cells correlated with the IOD (Fig. S12); but for Africa the areas of positive and negative correlations are similar. TMCFs, evergreen broadleaf forests and deciduous broadleaf forests show the largest % area with negative correlations; but for the IOD the majority of correlations is positive.

3.2.5. Trends and variability NDVI

TMCFs in Asia have the highest NDVI values, those in Africa the lowest. NDVI time series averaged over all TMCFs show a significant positive trend; this trend is explained by positive trends in the Americas and in Asia; however, there is no significant average trend for the African TMCFs (Ta-

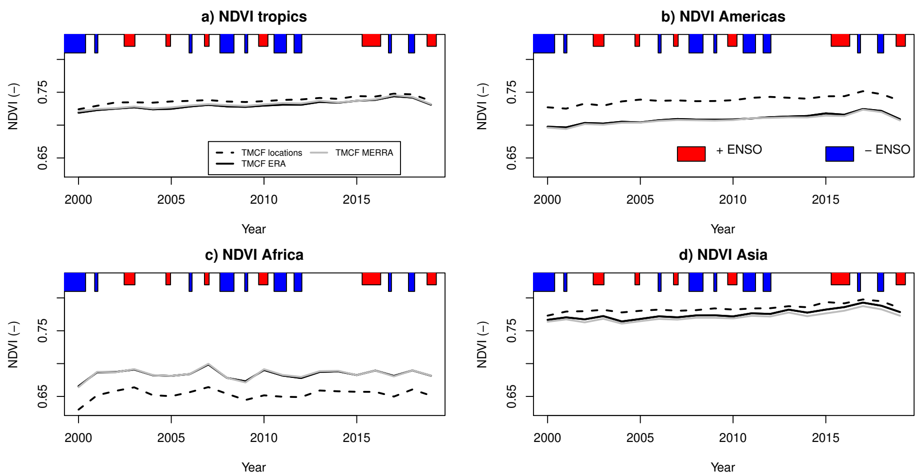

Figure 12: Same as Fig. 4 but for NDVI from 2000 until 2019. No significant sign tests or significant correlations are found between NDVI and ONI or between NDVI and ENSO.

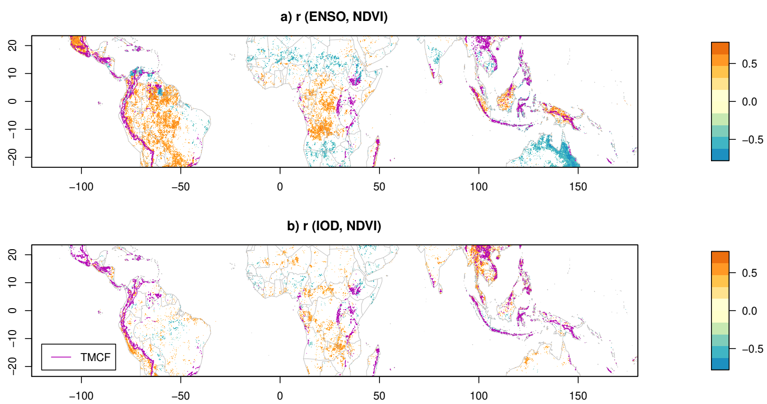

Figure 13: Same as Fig. 5 but for NDVI. More areas show a significant correlation with ENSO than with the IOD; throughout the tropics TMCFs and evergreen broadleaf forest have the largest % area affected (Fig. S13).

ble 5, S4). More TMCF areas have significant correlations of NDVI with ENSO than with the IOD; although the number of areas with significant correlations is smaller than that for temperature, cloud-base height and pre-

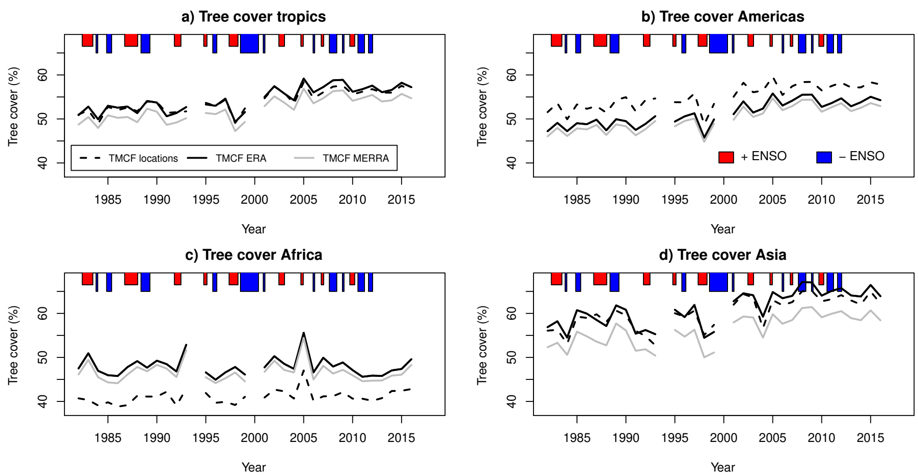

Figure 14: Same as Fig. 4 but for MEaSUREs tree-cover fraction from 1982–2016; 1994 and 2000 are not included because of poor data coverage (Song et al., 2018). No significant sign tests or significant correlations are found between tree cover and ONI.

cipitation. The number of positive correlations is larger than the number of negative correlations. The average time series show no significant correlations with either ENSO or the ONI.

3.2.6. Trends and variability in tree cover

Tree cover as defined in the MEaSUREs data set (Song et al., 2018) increases in TMCFs in the Americas, Asia and the entire tropics, but does not show a trend in Africa. For the Americas and Asia more areas show an increase in tree-cover over time than a decline. No significant association is found between changes in tree cover and the occurrence of ENSO events or between tree cover and strength of the ENSO signal. A limitation of the

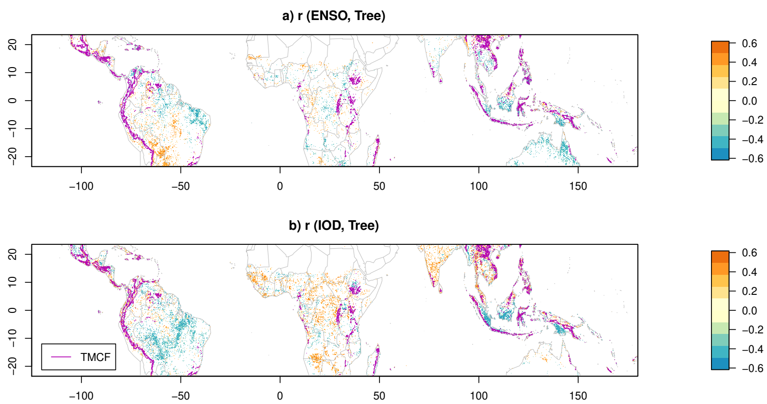

Figure 15: Same as Fig. 5 but for % tree cover. A small percentage area shows a significant correlation with either ENSO or the IOD (Fig. S14), however in some areas where deforestation rates are high (southern parts of the Amazon in Brazil, South Borneo, West Sumatra) negative correlations between tree cover and either ENSO or the IOD are found.

MEaSUREs data set is that it does not provide information about the type of tree cover.

The percentage of areas with significant correlations of tree-cover and either ENSO and IOD is small; however a higher density of pixels with significant correlations can be found in areas where deforestation rates are high (Fig. 15.

3.2.7. Summary trend and variability analysis

Trend analysis showed that over the past decades while temperatures in TMCFs increased as a result of global warming, the increase was on average smaller than for other tropical land-cover types. There is mixed evidence for TMCFs becoming drier; in the American TMCFs a significant negative trend was found in the TRMM precipitation data but for other continents no change was found in the averaged TRMM precipitation. Cloud-base height averaged over all TMCFs decreased, leading on average to wetter conditions; however, for some regions, in particular in the Americas, the cloud-base height increased. Outside the TMCFs, the increase in cloud-base height was large in the interiors of South America and Africa and it is an open question if the lifting of the cloud base will extend to the adjacent TMCFs in the future. TMCFs, on average, tend to become greener; this was evidenced both by an average increase in NDVI and in tree-cover. There are, however, important exceptions in particular in Africa – the average NDVI and tree cover for the continent did not show a significant trend; areas with positive and negative trends were similarly large and trends cancelled each other out. For the entire tropics, a larger proportion of TMCFs showed and increase in tree cover whereas for evergreen broadleaf forests the areas with positive and negative changes were similar in size. NDVI did increase on average in both; this positive trend was smaller in evergreen broadleaf vegetation than in TMCFs in the Americas and Asia, but was larger in Africa (Table 5).

A link was found between climate oscillators, IOD and ENSO and the climate of TMCFs. For most of the TMCFs, temperature was positively correlated to the IOD. Positive associations with ENSO occurred over fewer areas for some of the TMCFs in the Americas and Asia. Conditions tend to be drier during warm ENSO events in American TMCFs because of a reduction in rainfall and in Asian TMCFs both because of a reduction in rainfall and a lifting of the cloud-base. For African TMCFs, the effects were much less pronounced, but there was a tendency for the cloud-base height to decrease over TMCFs in eastern regions and to lift in central regions. The effect on vegetation greenness and tree cover associated with ENSO and IOD variations was much smaller, and some cases opposite to that noticed in precipitation.

3.3. Sensitivity of land-cover classification to an arbitrary increase in T_{2m} and $T_{d,2m}$

The sensitivity of the Random Forest Classifier is explored by modelling the response to a change in climate that is in line with the 'lifting cloud-base hypothesis'. Using the Random Forest Classifier, the spatial extent of TMCFs (and of other land-cover classes) is predicted for an increase in temperature by 1 K and an increase in cloud base-height by 100 m, which corresponds to an increase in $T_{d,2m}$ of 0.25 K. This sensitivity analysis provides an indication of the stability of the classification and indicates the direction of change of land-cover when exposed to a warmer, drier climate. The adopted approach does not address the response of individual species to a warming event; such an approach would provide a more realistic projection as to how the composition of biomes is affected. One limitation of the adopted approach is, for example, that it is not possible to simulate the composition of biomes not in existence under current conditions such as non-analogue species assemblages which have been observed in response to past glaciations (Street-Perrott et al., 2007).

The results of the sensitivity analysis are shown in Fig. 16. The effect of a change in temperature and cloud-base height on the classification is smallest in the Americas and highest in Africa and Asia. A proportion of TMCF cells in Africa and the Americas move into one or more of the drier classes (predominantly deciduous broadleaf and savanna). In Asia the same shift occurs, but here the loss of TMCF cells is more than compensated for by a movement of evergreen broadleaf forests into the TMCFs. Hence the lifting of the cloud base has the potential to reduce the spatial extent of TMCFs in some areas, e.g. in Africa, and expand it in others, in particular in Asia. The change in altitude of TMCFs showed a divergent pattern; at lower altitudes,

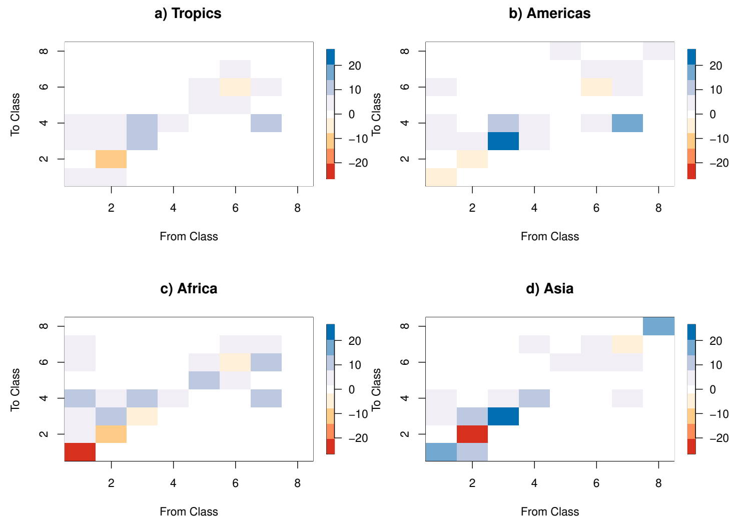

Figure 16: Sensitivity analysis of the Random Forest classification in response to a 1 K increase in temperature and a 100 m increase in cloud-base height. The diagonal shows the overall percentage change: positive numbers indicate the land cover class has increased in size, negative numbers that it has decreased. Off diagonal numbers in the columns show the increase of the new land-cover class.

below 1000 m a.s.l. (Asia and Americas) or 2000 m. a.s.l (Africa), TMCFs on average moved upward whereas at altitudes above 4000 m a.s.l. (Americas) or 2000 m. a.s.l. (Asia) TMCFs moved downward (not shown).

4. Discussion

The aim of the present study is to estimate the spatial distribution of TMCFs and to investigate how their climate, vegetation greenness and tree-cover fraction have changed during the past 20 to 40 years. An important aspect of this analysis is the use of ERA5-Land and MERRA-2 reanalysis temperature, dew-point temperature and cloud-base height to obtain information about conditions favourable for TMCFs. Reanalysis uses physical representations of the atmosphere to estimate the spatial and temporal distribution of meteorological variables globally including areas where no measurements are available. The availability of reanalysis at higher spatial resolutions than before offers the prospect of obtaining information relevant at more local scales.

4.1. Random Forest classification results

The Random Forest classifier (Breiman, 2001; Liaw and Wiener, 2002) was informed by a range of data sets, directly or indirectly linked to the humid conditions of TMCFs (Grubb and Whitmore, 1966; Aldrich et al., 1997; Bruijnzeel et al., 2011), to obtain estimates of their spatial distribution. The data used were altitude, slope, relief, distance from the coast and seasonal statistics (monthly minimum, mean and maximum) of NDVI, temperature, dewpoint temperature, cloud-base height and precipitation (predominantly rainfall and excluding occult precipitation).

For the identification of TMCFs, relief and slope were the two most important variables. This indicates that the uplift of air, forced by orography, and associated increase in humidity leading to more frequent supersaturated conditions and occurrence of fog and low-level clouds is a key factor in determining the location of TMCFs. Other important variables are measures of NDVI seasonality and of spatial variability in NDVI; these measures are the most important for the identification of evergreen broadleaf forests as well as for the other IGBP land-cover types. Use of reanalysis temperature, dew-point temperature and cloud-base height improved the classification results of TMCFs but, rather surprisingly, also those of grasslands and crops. This latter result is intriguing and suggests that conversion of natural cover into grass land or crops affects temperatures and humidity of the overlying atmosphere (Sagan et al., 1979; Pielke Sr et al., 2007). The improvement of the classification by incorporation of climate data emphasizes the link between climate and vegetation that has been long recognized, e.g. in the studies by Köppen (Belda et al., 2014) and early attempts to model biome primary productivity (Lieth, 1975).

The total TMCF area estimated, 2.1 x 10^6 km^2 $\pm$ 0.5 x 10^6 km^2, is at the upper end of previous estimates. The variables most important for the identification of TMCFs (measures of orography, NDVI, temperature and cloud-base height), are, with the exception of NDVI, not directly affected by humans. Hence it is probable that in some cases the classifier has identified potential TMCF locations rather than actual ones, e.g. in the Andes and in Africa there is ample evidence that humans have affected forests, including TMCFs, for centuries (Bush et al., 2008; Di Pasquale et al., 2008; Feeley et al., 2011; Sylvester et al., 2017; Marchant et al., 2018).

Our approach to identify TMCFs has similarities to the study by Mulligan and Burke (2005) that identified 'cloud affected' montane forests. The latter study used cloud frequency observed from satellite and cloud-base height (referred to as lifting condensation level) from a 1 km climatology based on spatial interpolation of station data (Hijmans et al., 2005). The agreement between the TMCF area for 25 countries estimated in the present study and in the study by Mulligan and Burke (2005) was good for the Americas and Asia, but not for Africa; here Mulligan and Burke (2005) estimated a much larger extent of 'cloud affected' montane forests. Possible explanations for this difference are 1) that the reanalysis used in the present study shows drier conditions over Africa and higher cloud-base height values than those used in Mulligan and Burke (2005) or 2) that the RF classifier used in the present study is constrained by training sites distributed across Africa that indicate a non-TMCF class; as a result of which the classification obtains clusters of TMCFs located closely to the training sites identified by Aldrich et al. (1997). It is worth noting that both studies identify the potential for a large presence of TMCFs in Ethiopia, despite this region having a modest presence in the Aldrich et al. (1997) data. In the Ethiopian highlands, a large proportion of old-growth forests has disappeared and has been replaced by crop land and tree plantations (Dessie and Kleman, 2007; Kidane et al., 2012).

TMCFs environments differ between continents. In Africa, TMCFs tend to be drier, rainfall and atmospheric humidity are lower and the distance to the coast is larger, and indications are that they are more patchy as well — NDVI values are lower and spatially more variable than in other continents, furthermore the probability of their occurrence estimated by the RF classifier is lower and the proportion of crop land is higher. TMCFs in Asia appear warmer and are located at lower altitudes than in other continents.

4.2. Detection of trends in temperature, cloud-base height, precipitation NDVI and tree cover

Because of the relatively low resolution of the data, $0.1° \times 0.1°$, the change detection was focused on the identification of regional, rather than local pressures on TMCFs. We analysed changes in TMCF temperature, cloud-base height, NDVI and tree cover and found large differences among and within continents.

Climate change potentially poses a threat to the future existence of TMCFs; its most important adverse effects are linked to increased temperatures and to decreased precipitation. We found ample evidence for increased temperatures in TMCFs over the past 40 years, although the rate of increase was lower than for many other tropical land-cover classes. Species will either have to adapt to warmer conditions or move to higher altitudes. Evidence for upward movement of tree species in response to global warming has been found in the Andes for example (Feeley et al., 2011). This upward movement has been found for extended periods during the Holocene as well (Bush et al., 2005, 2008; Di Pasquale et al., 2008). A second, potentially more serious effect is that the cloud base may be elevated in response to global warming and that occult precipitation, which is an important source of water for TMCFs, is diminished as a result. This 'lifting cloud-base hypothesis' was analyzed using ERA5-Land and MERRA-2 cloud-base height of the past four decades. It was found that surface-air temperature averaged over all TMCFs increased, however, dew-point temperature increased as well. In the Americas the increase in dew-point temperature was smaller than in surface-air temperature, resulting in an overall increase in cloud-base height over time in agreement with the 'lifting cloud-base hypothesis'. In Asia and parts of Africa, dewpoint temperatures increased more than surface-air temperatures, leading to a decrease in cloud-base height; about twice as many areas showed a decrease in cloud-base height compared to an increase (Table S5). Locally there are important exceptions to this trend, e.g. in several East African TMCFs cloud-base height increases leading to a reduction in occult precipitation (Cuní-Sanchez et al., 2018; Los et al., 2019). The decrease in occult precipitation poses a problem for these TMCFs since in Africa, compared to other continents, TMCFs are drier and their dependency on occult precipitation is greater. Cloud-base height changed in different ways across the tropics. For the interiors of South America and Africa, the cloud-base height increased substantially (up to 400 m in 40 years) whereas in tropical Asia cloud-base height decreased. TMCFs in Asia are by and large located on islands, suggesting a control of the ocean on the observed increase of atmospheric humidity (Chen and Liu, 2016) and higher dew-point temperatures. A caveat is that the increase in dewpoint temperature for an important part the result of the bias correction of the reanalyses which is based on station data (Table S5). The correction affects the ERA5-Land products more than the MERRA-2 products. Trends in TRMM precipitation between 2000 and 2019 tended to be local, whereas changes in cloud-base height were noticeable when averaged over continents and appeared a more important factor affecting water inputs into TMCFs.

MEaSUREs tree-cover data (Song et al., 2018) declined between 1982 and 2016 in about half of the African TMCFs and increased in most of the remainder; the resulting average secular trend in all African TMCFs was not significant. Regional studies in Tanzania (Hamunyela et al., 2020) found that deforestation rates in montane forests are larger than rates of forest recovery — the MEaSUREs tree-cover data (Song et al., 2018) show a decline here as well. By contrast, both in the American and Asian TMCFs a net increase in tree cover between 1982 and 2106 was found, although about 20 % of TMCFs in both regions showed a decline. The MEaSUREs data set (Song et al., 2018) has been tested extensively and is suitable for change detection, however it does not distinguish between tree-cover types and hence it is not possible to conclude whether the increases in forest cover in the tropics are linked to an increase in natural vegetation or to an increase in agroforestry. Similar to tree cover, average MODIS NDVI (2000–2019) in African TMCFs did not show a significant trend but did increase in American and Asian

TMCFs. Increased NDVI has been attributed to elevated atmospheric CO_2 concentrations — the attribution varies between 40 % to 70 % (Los, 2013; Zhu et al., 2016), to increased temperatures in mid-to-high latitudes (Myneni et al., 1997; Slayback et al., 2003) and at higher altitudes (Wang et al., 2011). These effects could also contribute to an increase in tree-cover, in particular at higher elevations. In addition, Song et al. (2018) attributed 60 % of increased tree cover world-wide to land-cover change and forest restoration. Evergreen broadleaf forests did not see a net increase (with the exception of Asia), hence our results are different from previous analyses where the decline in tree cover in TMCFs was higher than in other tropical forests (FAO, 1995; Doumenge et al., 1995; Mulligan and Burke, 2005). Potential explanations for this are (1) the remoteness of TMCFs (Mulligan, 2010; Bruijnzeel et al., 2011; Hamunyela et al., 2020); this, combined with the sometimes hostile climate, the less accessible terrain, and deforestation legislation preventing felling on slopes above a certain gradient, make it more difficult for large scale conversion of TMCFs than for lowland forests (2) replacement of original forests or reforesting of areas with tree plantations to provide timber and fuel (Dessie and Kleman, 2007; Martínez et al., 2009; Kidane et al., 2012) (3) global change (temperature and atmospheric CO_2) which in some areas results in an upward movement of trees and stimulation of tree growth (Feeley et al., 2011), and (4) a greater appreciation of the ecosystem services provided by TMCFs and the establishment of incentive schemes for their conservation (Asquith et al., 2008; Muñoz-Piña et al., 2008; Van Hecken et al., 2012).

4.3. Climate oscillators

Climate oscillators, ENSO and IOD, affect large parts of the tropics and are of importance for the climate of TMCFs. ENSO is more closely linked to rainfall variability in TMCFs than the IOD across the tropics; for the west coast of the Americas and in Asia, warm (cold) ENSOs are associated with a decrease (increase) in rainfall (Ropelewski and Halpert, 1987; Saji and Yamagata, 2003). ENSO and the IOD have an equally large effect on rainfall in African TMCFs; a positive phase of the IOD is associated with increased rainfall, whereas a warm ENSO depresses rainfall. For most TMCFs, the IOD is more strongly associated with variations in surface-air temperature and dewpoint temperature than ENSO; the relationship of the IOD and temperature or dewpoint temperature is predominantly positive. ENSO and IOD affect cloud-base height in TMCFs for a similar percentage of area; however the sign of the relationship varies from one continent to the next.

The relationship between climate oscillators and NDVI or tree cover is less clear than that for precipitation and cloud-base height. For most TMCFs and tropical evergreen broadleaf forests NDVI values are not affected, even during periods with less rainfall. For areas that show a significant correlation, NDVI in TMCFs tends to be positively correlated with ENSO — this positive relationship is consistent for all continents and is unlikely to be caused by a decrease in rainfall but could be linked with a reduction in cloud cover, more suitable illumination conditions and a less contaminated observation by the satellite sensor (Morton et al., 2014). Some regions in the Americas, notably the southern edge of the Amazon, and in Asia show a negative correlation between ENSO and tree-cover. Drier conditions in these areas during warm ENSO events favour forest clearing and biomass burning — increases in forest fires and clearing during warm ENSO events have been reported elsewhere (Malingreau et al., 1985; Mori, 2000; Achard et al., 2002; Lewis et al., 2011).

4.4. Response to imposed 'lifting cloud base'

Climate models show a lifting of the cloud base that will reduce the amount of occult precipitation that TMCFs receive (Still et al., 1999). The effect of an idealized hypothetical 1 K warming and lifting of the cloud base by 100 m, on the spatial distribution of TMCFs was explored; this showed a reduction in their extent in the Americas and Africa. The outcome for Asia, however, was different since here the reduction in TMCF area is more than compensated for by a shift of broadleaf evergreen vegetation into TMCFs — hence a hypothesized lifting of the cloud base associated with climate change may not lead to a reduction in the extent of TMCFs in Asia. The analysis of past climates of the last 30,000 years also indicates that the response of TMCFs in the three major tropical regions was different. At the Last Glacial Maximum (LGM), in the wettest parts of the Australasian "Maritime Continent" and South America, cloud-adapted upper-montane taxa migrated downslope into areas currently occupied by EBLs (Flenley, 1998). By contrast, in drier parts of Africa, the corresponding montane elements were restricted to scattered pockets at lower elevations, in association with C_4 graminoids and savanna/xerophytic trees and shrubs, forming plant communities that have no modern counterparts (Street-Perrott et al., 2007; Los et al., 2019). TMCFs and mountain forests are more vulnerable in the larger and more ancient cratonic continent of Africa compared to the other continents, since mountains tend to be much more isolated, and TMCFs are often surrounded by dry forests and savannas (Bussmann, 2002). This is not the case in the tectonically more active and more continuous mountain ranges of Asia and South America, where TMCFs are more closely spaced.

5. Conclusions

The ERA5-Land and MERRA-2 reanalysis temperature and dewpoint temperature provide useful information that improves the classification of TMCFs and allow analysis of variations in their temperature, dewpoint temperature and cloud-base height.

We estimate that TMCFs cover about 4 % ±1 % of the tropical land surface; this estimate is at the upper end of previous estimates and probably includes areas where tree cover has been reduced or has been replaced by tree plantations.

Evidence of significant warming of TMCFs was found in all continents (0.15 °C y^{-1} – 0.23 °C y^{-1}); however, the amount of warming was higher for most other tropical land-cover types.

Testing of the 'lifting cloud-base hypothesis' with ERA5-Land and MERRA-2 reanalyses of the past 40 years showed that it is valid for TMCFs in the Americas and to a lesser extent in Africa, but for TMCFs in Asia cloud-base height decreased because $T_{d,2m}$ increased more than $T_{2,m}$ due to the (counter-intuitive) effects of increasing atmospheric moisture.

Changes in TMCF tree cover were less unidirectional than previously thought; areas with reduced tree cover were found in all continents, however in the Americas and Asia more TMCFs showed a gain in tree cover. TMCFs with tree loss in Africa were of a similar extent to those showing a gain in tree cover. The data used did not provide information on the type of tree cover (natural versus agro-forestry) and there is evidence from the literature that locally, tree plantations explain a substantial part of this increase.

ENSO signals were dominant, compared to IOD signals, in TRMM precipitation of American and Asian TMCFs, whereas the reverse was found for temperature and dewpoint temperature in TMCFs across the tropics. ENSO and IOD signals were approximately equally important for precipitation in African TMCFs and for cloud-base height in TMCFs across the tropics.

The RF classifier projects that a hypothetical lifting of the cloud base by 100 m throughout the tropics would reduce the spatial extent of TMCFs in the Americas and in particular in Africa, but would increase it in Asia. A high sensitivity of African TMCFs to climate change is supported by longer-term evidence reported in palaeoecological studies .

Acknowledgements

We are grateful for all efforts made by investigators to put the data sets used in this study in the public domain. We thank three anonymous reviewers for their detailed, in-depth comments to improve the manuscript.

References

Achard, F., Eva, H.D., Stibig, H.J., Mayaux, P., Gallego, J., Richards, T., Malingreau, J.P., 2002. Determination of deforestation rates of the world's humid tropical forests. Science 297. 999–1002, doi: 10.1126/science.1070656.

Aldrich, M., Billington, C., Edwards, M., Laidlaw, R., 1997. Tropical montane cloud forests: An urgent priority for conservation. WCMC Biodiversity Bulletin 2.

Asquith, N.M., Vargas, M.T., Wunder, S., 2008. Selling two environmental services: In-kind payments for bird habitat and watershed protection in Los Negros, Bolivia. Ecol. Econ. 65, 675–684, doi: 10.1016/j.ecolecon.2007.12.014.

Belda, M., Holtanová, E., Halenka, T., J, K., 2014. Climate classification revisited: from Köppen to Trewartha. Clim. Res. 59, 1–13, doi: 10.3354/cr01204.

Bradley, R.S., Keimig, F.T., Diaz, H.F., 2004. Projected temperature changes along the American cordillera and the planned GCOS network. Geophys. Res. Lett. 31, L16210, doi: 10.1029/2004GL020229.

Breiman, L., 2001. Random forests. Mach. Learn. 45, 5–32, doi: 10.1023/A:1010933404324.

Bruijnzeel, L.A., Mulligan, M., Scatena, F.N., 2011. Hydrometeorology of tropical montane cloud forests: emerging patterns. Hydrol. Process. 25, 465–498, doi: 10.1002/hyp.7974.

Bruijnzeel, L.A., Scatena, F.N., Hamilton, L.S., 2010. Tropical Montane Cloud Forests. Science for Conservation and Management. Cambridge University Press, Cambridge, UK.

Bubb, P., May, I., Miles, L., Sayer, J., 2004. Cloud Forest Agenda. volume 20 of *NEP-WCMC Biodiversity Series*. UNEP-WCMC, Cambridge.

Bush, M.B., Hanselman, J.A., Hooghiemstra, H., 2011. Andean montane forests and climate change. second ed.. Springer-Verlag, Berlin Heidelberg. Tropical Rainforest Responses to Climatic Change Chapter 2. pp. 35–60.

Bush, M.B., Hansen, B.C.S., Rodbell, D.T., Seltzer, G.O., Young, K.R., León, B., Abbott, M.B., Silman, M.R., Gosling, W.D., 2005. A 17 000-

year history of andean climate and vegetation change from Laguna de Chochos, Peru. J. Quat. Sci. 20, 703–714, doi: 10.1002/jqs.983.

Bush, M.B., Silman, M.R., McMichael, C., Saatchi, S., 2008. Fire, climate change and biodiversity in Amazonia: a late-holocene perspective. Philos. Trans. R. Soc. Lond., B, Biol. Sci. 363, 1795–1802, doi: 10.1098/rstb.2007.0014.

Bussmann, R.W., 2002. Islands in the desert — Forest vegetation of Kenya's smaller mountains and highland areas (Nyiru, Ndoto, Kulal, Marsabit, Loroghi, Ndare, Mukogodo, Porror, Mathews, Gakoe, Imenti, Ngaia, Nyambeni, Loita, Nguruman, Nairobi). J. East Afr. Nat. Hist. 91, 27–79.

Cavelier, J., 1996. Tropical Forest Plant Ecophysiology. International Thomson Publishing, Florence, Kentucky 41042, USA. chapter Environmental factors and ecophysiological processes along altitudinal gradients in wet tropical mountains. 14, pp. 399–439, doi: 10.1007/978–1–4613–1163–8_14.

Chen, B., Liu, Z., 2016. Global water vapor variability and trend from the latest 36 year (1979 to 2014) data of ECMWF and NCEP reanalyses, radiosonde, GPS, and microwave satellite. J.Geophys. Res. Atmos. 121, 11,442–11,462, doi: 10.1002/2016JD024917.

Copernicus Climate Change Service (C3S), 2017. ERA5: Fifth generation of ECMWF atmospheric reanalyses of the global climate. Copernicus Climate Change Service Climate Data Store (CDS) , url: https://cds.climate.copernicus.eu/cdsapp#!/home (accessed 01–2020).

Copernicus Climate Change Service (C3S), 2019. C3S ERA5-land reanalysis. Copernicus Climate Change Service Climate Data Store (CDS) , url: https://cds.climate.copernicus.eu/cdsapp#!/home (accessed 01–2020).

Cuní-Sanchez, A., Omeney, P., Pfeifer, M., Olaka, L., Boru Mamo, M., Marchant, R., Burgess, N.D., 2018. Climate change and pastoralists: perceptions and adaptation in montane Kenya. Clim. Dev. , 1–12, doi: 10.1080/17565529.2018.1454880.

Danielson, J.J., Gesch, D.B., 2011. Global multi-resolution terrain elevation data 2010 (GMTED2010). Technical Report. USGS. Earth Resources Observation and Science (EROS), United States Geological Survey, Sioux Falls, South Dakota, USA.

Dessie, G., Kleman, J., 2007. Pattern and magnitude of deforestation in the south central Rift Valley region of Ethiopia. Mt. Res. Dev. 27, 162–168, doi: 10.1659/mrd.0730.

Di Pasquale, G., Marziano, M., Impagliazzo, S., Lubritto, C., De Natale, A., Bader, M.Y., 2008. The holocene treeline in the northern Andes (Ecuador): First evidence from soil charcoal. Palaeo 259, 17–34, doi: 10.1016/j.palaeo.2006.12.016.

Diaz, H.F., Bradley, R.S., Ning, L., 2014. Climatic changes in mountain regions of the American Cordillera and the tropics: historical changes and future outlook. Arct. Antarct. Alp. Res. 46, 735–743, doi: 10.1657/1938–4246–46.4.735.

Doumenge, C., Gilmour, D., Pérez, M.R., Blockhus, J., 1995. Tropical montane cloud forests: Conservation status and management issues, in: Hamilton, L.S., Juvik, J.O., Scatena, F.N. (Eds.), Tropical Montane Cloud Forests, Springer US, New York, NY. pp. 24–37.

Feeley, K.J., Silman, M.R., Bush, M.B., Farfan, W., Cabrera, K.G., Malhi, Y., Meir, P., Salinas Revilla, N., Quisiyupanqui, M.N.R., Saatchi, S., 2011. Upslope migration of Andean trees. J. Biogeogr. 38, 783–791. doi:10.1111/j.1365-2699.2010.02444.x.

Flenley, J.R., 1998. Tropical forests under the climates of the last 30,000 years. Clim. Change 39, 177–197, doi: 10.1023/A:1005367822750.

FAO – Food and Agricultural Organization, 1995. Forest Resources Assessment 1990 – Global Synthesis – FAO Forestry Paper 124. Technical Report. FAO. Rome, http://apps.fao.org/.

Foster, P., 2001. The potential negative impact of global climate change on tropical montane cloud forest. Earth Sci. Rev. 55, 73–106.

Friedl, M.A., Sulla-Menashe, D., Tan, B., Schneider, A., Ramankutty, N., Sibley, A., Huang, X.M., 2010. MODIS collection 5 global land cover: Algorithm refinements and characterization of new datasets. Remote Sens. Environ. 114, 168–182.

Fu, Q., Manabe, S., Johanson, C.M., 2011. On the warming in the tropical upper troposphere: Model versus observations. Geophys. Res. Lett. 38, L15704, doi:10.1029/2011GL048101.

Gelaro, R., McCarty, W., Suárez, M.J., Todling, R., Molod, A., Takacs, L., Randles, C andDarmenov, A., Bosilovich, M.G., Reichle, R., Wargan, K andCoy, L., Cullather, R., Draper, C., Akella, S., Buchard, V., Conaty, A., da Silva, A., Gu, W., Kim, G.K., Koster, R., Lucchesi, R., Merkova, D., Nielsen, J.E., Partyka, G., Pawson, S., Putman, W., Rienecker, M., Schubert, S.D., Sienkiewicz, M., Zhao, B., 2017. The Modern-Era Retrospective Analysis for Research and Applications, Version 2 (MERRA-2),. J. Clim. 30, 5419–5454.

Grubb, P.J., Whitmore, T.C., 1966. A comparison of montane and lowland rain forets in Ecuador: II. The climate and its effects on the distribution and physiognomy of the forests. J. Ecol. 54, 303–333, doi: 10.2307/2257951.

Hamilton, L.S., Juvik, J.O., Scatena, F.N., 1995. The puerto rico tropical cloud forest symposium: Introduction and workshop synthesis, in: Hamilton, L.S., Juvik, J.O., Scatena, F.N. (Eds.), Tropical Montane Cloud Forests, Springer US, New York, NY. pp. 1–18.

Hamunyela, E., Brandt, P., Shirima, D., Do, H.T.T., Herold, M., Roman-Cuesta, R.M., 2020. Space-time detection of deforestation, forest degradation and regeneration in montane forests of Eastern Tanzania. Int. J. Appl. Eearth Obs. Geoinf. 88. doi:10.1016/j.jag.2020.102063.

Helmer, E.H., Gerson, E.A., Scott Baggett, L., Bird, B.J., Ruzycki, S., Vogesser, S.M., 2019. Neotropical cloud forests and páramo to contract and dry from declines in cloud immersion and frost. PLOS One , e0213155 doi: 10.1371/journal.pone.0213155.

Hemp, A., 2009. Climate change and its impact on the forests of Kilimanjaro. Afr. J. Ecol. 47, 3–10, doi: 10.1111/j.1365–2028.2008.01043.x.

Hijmans, R.J., 2019. Raster: Geographic Data Analysis and Modeling. URL: `https://CRAN.R-project.org/package=raster`. r package version 3.0-2.

Hijmans, R.J., Cameron, S.E., Parra, J.L., Jones, P.G., Jarvis, A., 2005. Very high resolution interpolated climate surfaces for global land areas. Int. J. Climatol. 25, 1965–1978, doi: 10.1002/joc.1276.

Huang, B., Thorne, P.W., Banzon, V.F., Boyer, T., Chepurin, G., Lawrimore, J.H., Menne, M.J., Smith, T.M., Vose, R.S., Zhang, H., 2017. Extended reconstructed sea surface temperature, version 5 (ERSSTv5): Upgrades, validations, and intercomparisons. J. Clim. 30, 8179–8205, doi: 10.1175/JCLI–D–16–0836.1.

Huete, A., Didan, K., Miura, T., Rodriguez, E.P., Gao, X., Ferreira, L.G., 2002. Overview of the radiometric and biophysical performance of the modis vegetation indices. Remote Sens. Environ. 83, 195–213.

Huffman, G.J., Adler, R.F., Bolvin, D.T., Gu, G., Nelkin, E.J., Bowman, K.P., Hong, Y., Stocker, E.F., Wolff, D.B., 2007. The TRMM multi-satellite precipitation analysis: Quasi-global, multi-year, combined-sensor precipitation estimates at fine scale. J. Hydrometeorol. 8, 38–55, doi: 10.1175/JHM560.1.

Huffman, G.J., Adler, R.F., Bolvin, D.T., Nelkin, E.J., 2010. Satellite Rainfall Applications for Surface Hydrology. Springer Verlag, Heidelberg, Germany. chapter 1. The TRMM Multi-satellite Precipitation Analysis (TMPA), doi: 10.1007/978-90-481-2915-7.

Jarvis, A., Mulligan, M., 2011. The climate of cloud forests. Hydrol.Process. 25, 327–343, doi: 10.1002/hyp.7847.

Karmalkar, A.V., Bradley, R.S., Diaz, H.F., 2008. Climate change scenario for Costa Rican montane forests. Geophys. Res. Lett. 35, L11702, doi: 10.1029/2008GL033940.

Kidane, Y.O., Stahlmann, R., Beierkuhnlein, C., 2012. Vegetation dynamics, and land use and land cover change in the Bale Mountains, Ethiopia. Environ. Monit. Assess. 12, 7473–7489, doi: 10.1007/s10661–011–2514–8.

Lawrence, M.G., 2005. The relationship between relative humidity and the dewpoint temperature in moist air: A simple conversion and applications. Bull. Am. Meteorol. Soc. 86, 225–233, doi: 10.1175/BAMS–86–2–225.

Lewis, S.L., Brando, P.M., Phillips, O.L., van der Heijden, G.M.F., Nepstad, D., 2011. The 2010 amazon drought. Science 331, 554, doi: 10.1126/science.1200807.

Liaw, A., Wiener, M., 2002. Classification and regression by randomforest. R News 2, 18–22. URL: `htpps://CRAN.R-project.org/doc/Rnews/`.

Lieth, H., 1975. Primary Productivity of the Biosphere. Springer Verlag, Berlin, Heidelberg and New York. chapter Modelling primary productivity of the world. Ecol. Studies 14, pp. 237–263.

Lister, B.C., Garcia, A., 2018. Climate-driven declines in arthropod abundance restructure a rainforest food web. PNAS 115, E10397–E10406, doi: 0.1073/pnas.1722477115.

Los, S.O., 2013. Analysis of trends in fused AVHRR and MODIS NDVI data for 1982–2006: Indication for a CO_2 fertilization effect in global vegetation. Global Biogeochem. Cycles 27, 318–330, doi: 10.1002/gbc.20027.

Los, S.O., Collatz, G.J., Sellers, P.J., Malmstrom, C.M., Pollack, N.H., De-

Fries, R.S., Bounoua, L., Parris, M.T., Tucker, C.J., Dazlich, D.A., 2000. A global 9-yr biophysical land surface dataset from NOAA AVHRR data. J. Hydrometeorol. 1, 183–199.

Los, S.O., Street-Perrott, F.A., Loader, N.J., Froyd, C.A., Cuní-Sanchez, A., Marchant, R.A., 2019. Sensitivity of a tropical montane cloud forest to climate change, present, past and future: Mt. Marsabit, N. Kenya. Quat. Sci. Rev. 218, 34–48, doi: 10.1016/j.quascirev.2019.06.016.

Malingreau, J.P., Stephens, G., Fellows, L., 1985. Remote sensing of forest fires: Kalimantan and North Borneo in 1982–83. Ambio 14, 314–321.

Marchant, R., Richer, S., Boles, O., Capitani, C., Courtney-Mustaphi, C.J., Lane, P., Prendergast, M.E., Stump, D., De Cort, G., Kaplan, J.O., Phelps, L., Kay, A., Olago, D., Petek, N., Platts, P.J., Punwong, P., Widgren, M., Wynne-Jones, S., Ferro-Vázquez, C., Benard, J., Boivin, N., Crowther, A., Cuní-Sanchez, A., Deere, N.J., Ekblom, A., Farmer, J., Finch, J., Fuller, D., Gaillard-Lemdahl, M.J., Gillson, L., Githumbi, E., Kabora, T., Kariuki, R., Kinyanjui, R., Kyazike, E., Lang, C., Lejju, J., Morrison, K.D., Muiruri, V., Mumbi, C., Muthoni, R., Muzuka, A., Ndiema, E., Kabonyi Nzabandora, C., Onjala, I., Schrijver, A.P., Rucina, S., Shoemaker, A., Thornton-Barnett, S., van der Plas, G., Watson, E.E., Williamson, D., Wright, D., 2018. Drivers and trajectories of land-cover change in east africa: Human and environmental interactions from 6000 years ago to present. Earth Sci. Rev. 178, 322 – 378, doi: 10.1016/j.earscirev.2017.12.010.

Martínez, M.L., Pérez-Maqueo, O., Vázquez, G., Castillo-Campos, G., García-Franco, J., Mehltreter, K., Equihua, M., Landgrave, R., 2009. Effects of land use change on biodiversity and ecosystem serices in tropical montane cloud forests of Mexico. For. Ecol. Manag. 258, 1856–1863, doi: 10.1016/j.foreco.2009.02.023.

Mori, T., 2000. Effects of Droughts and Forest Fires on Dipterocarp Forest in East Kalimantan. Springer Japan, Tokyo. pp. 29–45, doi: 10.1007/978–4–431–67911–0_3.

Morton, D.C., Nagol, J., Carabajal, C.C., Rosette, J., Palace, M., Cook, B.D., Vermote, E.F., Harding, D.J., North, P.R.J., 2014. Amazon forests maintain consistent canopy structure and greenness during the dry season. Nature 506, 221–224, doi: 10.1038/nature13006.

Mulligan, M., 2010. Tropical Montane Cloud Forests. Cambridge University

Press. chapter Modelling the tropics-wide extent and distribution of cloud forest and cloud forest loss, with implications for conservation priority. International Hydrology Series, pp. 14–38.

Mulligan, M., Burke, S., 2005. DFID FRP Project ZF0216 Global cloud forests and environmental change in a hydrological context. Final Report. Technical Report. United Kingdom Department for International Development. http://www.ambiotek.com/cloudforests/cloudforest_finalrep.pdf.

Muñoz-Piña, C., Guevara, A., Torres, J.M., Braña, J., 2008. Paying for the hydrological services of Mexico's forests: Analysis, negotiations and results. Ecol. Econ. 65, 725–736, doi: 10.1016/j.ecolecon.2007.07.031. Payments for Environmental Services in Developing and Developed Countries.

Myneni, R.B., Keeling, C.D., Tucker, C.J., Asrar, G., Nemani, R.R., 1997. Increased plant growth in the northern high latitudes from 1981 to 1991. Nature 386, 698–702.

O'Gorman, P.A., Singh, M.S., 2013. Vertical structure of warming consistent with an upward shift in the middle and upper troposphere. Geophys. Res. Lett. 40, 1838–1842, doi: 10.1002/grl.50328.

Ohmura, A., 2012. Enhanced temperature varaibility in high-altitude climate change. Theor. Appl. Climatol. 110, 499–508, doi: 10.1007/s00704–012–0687–x.

Oliveira, R.S., Eller, C.B., Bittencourt, P.R.L., Mulligan, M., 2014. The hydroclimatic and ecophysiological basis of cloud forest distributions under current and projected climates. Ann. Bot. 113, 909–920, doi: 10.1093/aob/mcu060.

Philander, S.G., 1989. El Niño, La Niña and the Southern Oscillation.. volume 46 of *International Geophysics Series*. Academic Press, San Diego, California.

Pielke Sr, R.A., Adegoke, J., Beltrán-Przekurat, A., Hiemstra, C.A., Lin, J., Nair, U.S., Niyogi, D., Nobis, T.E., 2007. An overview of regional land-use and land-cover impacts on rainfall. Tellus 59B, 587–601, doi: 10.1111/j.1600–0889.2007.00251.x.

Pounds, J.A., Fogden, M.P.L., Campbell, J.H., 1999. Biological response to climate change on a tropical mountain. Nature 398, 611–615, doi: 10.1038/19297.

Power, M.J., Marlon, J., Ortiz, N., Bartlein, P.J., Harrison, S.P., Mayle, F.E., Ballouche, A., Bradshaw, R.H.W., Carcaillet, C., Cordova, C., Mooney, S., Moreno, P.I., Prentice, I.C., Thonicke, K., Tinner, W., Whitlock, C., Zhang, Y., Zhao, Y., Ali, A.A., Anderson, R.S., Beer, R., Behling, H., Briles, C., Brown, K.J., Brunelle, A., Bush, M., Camill, P., Chu, G.Q., Clark, J., Colombaroli, D., Connor, S., Daniau, A.L., Daniels, M., Dodson, J., Doughty, E., Edwards, M.E., Finsinger, W., Foster, D., Frechette, J., Gaillard, M.J., Gavin, D.G., Gobet, E., Haberle, S., Hallett, D.J., Higuera, P., Hope, G., Horn, S., Inoue, J., Kaltenrieder, P., Kennedy, L., Kong, Z.C., Larsen, C., Long, C.J., Lynch, J., Lynch, E.A., McGlone, M., Meeks, S., Mensing, S., Meyer, G., Minckley, T., Mohr, J., Nelson, D.M., New, J., Newnham, R., Noti, R., Oswald, W., Pierce, J., Richard, P.J.H., Rowe, C., Sanchez Goñi, M.F., Shuman, B.N., Takahara, H., Toney, J., Turney, C., Urrego-Sanchez, D.H., Umbanhowar, C., Vandergoes, M., Vanniere, B., Vescovi, E., Walsh, M., Wang, X., Williams, N., Wilmshurst, J., Zhang, J.H., 2008. Changes in fire regimes since the last glacial maximum: an assessment based on a global synthesis and analysis of charcoal data. Clim. Dyn. 30, 887–907, doi: 10.1007/s00382-007-0334-x.

Ropelewski, C.F., Halpert, M.S., 1987. Global and regional scale precipitation patterns associated with the El Niño/Southern Oscillation. Mon. Weather Rev. 115, 1606–1626, doi: 10.1175/1520–

0493(1987)115<1606:GARSPP>2.0.CO;2.

Sagan, C., Toon, O.B., Pollack, J.B., 1979. Anthropogenic albedo changes and the Earth's climate. Science 206, 1363–1368.

Saji, N.H., Goswami, B.N., Vinayachandran, P.N., Yamagata, T., 1999. A dipole mode in the tropical Indian Ocean. Nature 401, 360–363, doi: 10.1038/43854.

Saji, N.H., Yamagata, T., 2003. Possible impacts of Indian Ocean Dipole Mode events on global climate. Clim. Res. 25, 151–169, doi: 10.3354/cr025151.

Scatena, F.N., Bruijnzeel, L.A., Bupp, P., Das, S., 2010. Tropical Montane Cloud Forests. Science for Conservation and Management. Cambridge University Press, Cambridge, UK. chapter 1. Setting the stage.

Sellers, P.J., Los, S.O., Tucker, C.J., Justice, C.O., Dazlich, D.A., Collatz, G.J., Randall, D.A., 1996. A revised land-surface parameterization (SiB2) for atmospheric GCMs. Part 2: The generation of global fields of terrestrial biophysical parameters from satellite data. J. Clim. 9, 706–737.

Simpson, J., Adler, R.F., North, G.R., 1988. A proposed Tropical Rainfall

Measuring Mission (TRMM) satellite. Bull. Amer. Meteorol. Soc. 69, 278–295, doi: 10.1175/1520–0477(1988)069<0278:APTRMM>2.0.CO;2.

Slayback, D.A., Pinzon, J.E., Los, S.O., Tucker, C.J., 2003. Northern hemisphere photosynthetic trends 1982–99. Glob. Change Biol. 9, 1–15.

Smith, A.N., Lott, N., Vose, R., 2011. The integrated surface data base: Recent developments and partnerships. Bul. Am. Meteorol. Soc. 92, 704–708, doi:10.1175/2011BAMS3015.1.

Song, X., Hansen, M.C., Stehman, S.V., Potapov, P.V., Tyukavina, A., Vermote, E.F., Townshend, J.R., 2018. Global land change from 1982 to 2016. Nature 560, 639–643, doi: 10.1038/s41586–018–0411–9.

Still, C.J., Foster, P.N., Schneider, S.H., 1999. Simulating the effects of climate change on tropical montane forests. Nature 389, 608–610.

Street-Perrott, F.A., Barker, P.A., Swain, D.L., Ficken, K.J., Wooller, M.J., Olago, D.O., Huang, Y., 2007. Late Quaternary changes in ecosystems and carbon cycling on Mt. Kenya, East Africa: a landscape-ecological perspective based on multi-proxy lake-sediment influxes. Quat. Sci. Rev. 26, 1838–1860, doi: 10.1016/j.quascirev.2007.02.014.

Stumpf, R., Kuring, N., pers. comm. Distance from coastline at $0.01^\circ \times 0.01^\circ$ obtained from https://oceancolor.gsfc.nasa.gov (accessed mar 2020).

Subblette Mosblech, N.A., Chepstow-Lusty, A., Valencia, B.G., Bush, M.B., 2012. Anthropogenic control of late-Holocene landscapes in the Cuzco region, Peru. Holocene 22, 1361–1372, doi: 0.1177/0959683612449760.

Sulla-Menashe, D., Gray, J.M., Abercrombie, S.P., Friedl, M.A., 2019. Hierarchical mapping of annual global land cover 2001 to present: The modis collection 6 land cover product. Remote Sens. Environ. 222, 183–194, doi: 10.1016/j.rse.2018.12.013.

Sylvester, S.P., Heitkamp, F., Sylvester, M.D.P.V., Jungkunst, H.F., Sipman, H.J.M., Toivonen, J.M., Gonzales Inca, C.A., Ospina, J.C., Kessler, M., 2017. Relict high-andean ecosystems challenge our concepts of naturalness and human impact. Sci. Rep. 7, 3334, doi: 10.1038/s41598-017-03500-7.

Van Hecken, G., Bastiaensen, J., Vásquez, W., 2012. The viability of local payments for watershed services: Empirical evidence from Matiguás, Nicaragua. Ecol. Econ. 74, 169–176, doi: 10.1016/j.ecolecon.2011.12.016.

Wang, J., Ye, B., Liu, F., Li, J., Yang, G., 2011. Variations of ndvi over elevational zones during the past two decades and climatic controls in the qilian mountains, northwestern china. Arct. Antarct. Alp. Res. 43, 127–136, doi: 10.1657/1938–4246–43.1.127.

Wessel, P., Luis, J.F., 2017. The gmt/matlab toolbox. Geochem. Geophys. Geosyst. 18, 811–823.

Williams, J.W., Jackson, S.T., Kutzbach, J.F., 2007. Projected distributions of novel and disappearing climates by 2100 AD. PNAS 104, 5738–5742, doi: 10.1073/pnas.0606292104.

Zhu, Z., Piao, S., Myneni, R.B., Huang, M., Zeng, Z., Canadell, J.G., Ciais, P., Sitch, S., Friedlingstein, P., Arneth, A., Cao, C., Cheng, L., Kato, E., Koven, C., Li, Y., Lian, X., Liu, Y., Liu, R., Mao, J., Pan, Y., Peng, S., Peñuelas, J., Poulter, B., Pugh, T.A.M., Stocker, B.D., Viovy, N., Wang, X., Wang, Y., Xiao, Z., Yang, H., Zaehle, S., Zeng, N., 2016. Greening of the earth and its drivers. Nature Clim. Change 6, 791–795, doi:10.1038/nclimate3004.

Table 3: Assessment of the accuracy of the Random Forest Classification using the ERA5-Land T_{2m} and Z_C products. The diagonal of the confusion matrix shows the number of training sites correctly classified; the off-diagonal numbers show the type-1 and type-2 classification errors. The out-of-bag (OOB) estimate of error rate for the overall classification is 5.7 %. The column '% Error' shows the classification error per class, 'r MODIS' shows the correlation between the class probability estimated by the Random Forest Classifier and the % cover of the same class in the aggregated MODIS classification (Friedl et al., 2010; Sulla-Menashe et al., 2019), and '% Area' shows the percentage area per class as estimated by the Random Forest Classifier. (EBL = Evergreen broadleaf forest; DBL = Deciduous broadleaf forest; see also Table 2)

		Predicted Class										
		TMCF	**2**	**3**	**4**	**5**	**6**	**7**	**8**	% Error	r MODIS	% Area
Actual Class	1. TMCF	349	58	13	10	0	19	9	2	24		4.3
	2. EBL	36	952	10	1	0	0	0	0	5	0.93	20.3
	3. DBL	14	14	940	30	0	0	1	0	6	0.77	8.0
	4. SAV	9	2	29	935	0	14	10	0	6	0.82	20.9
	5. Shrub	0	0	0	0	956	26	0	4	3	0.87	5.6
	6. Grass	2	0	0	10	12	953	23	0	5	0.84	20.9
	7. Crop	1	0	0	34	0	33	932	0	7	0.70	5.5
	8. Barren	0	0	0	0	0	0	0	999	0	0.98	14.7

Table 4: Error estimates (η) of classifications not using T_{2m} and Z_C products (no reanalysis –η NR) and those using the ERA5-Land (η E) and MERRA-2 (η M) T_{2m} and Z_C products. Columns η E and η M are repeated from tables 3 and S2 for convenience. Errors in columns η E–M, η E–NR, and η M–NR represent the mean deviations between two classifications (e.g. η E–M indicates average of error ERA5-Land compared to MERRA-2 and the other way around). EBL = Evergreen broadleaf forest; DBL = Deciduous Broadleaf forest (Table 2).

Class	η NR (%)	η E (%)	η M (%)	η E–M (%)	η E–NR (%)	η M–NR (%)
1. TMCF	25.2	24.1	24.7	14.2	13.9	12.6
2. EBL	5.3	4.7	4.9	3.6	4.0	3.7
3. DBL	6.6	5.9	5.4	11.4	17.9	16.7
4. Savanna	7.0	6.4	6.4	5.3	8.5	8.4
5. Shrub	3.7	3.0	2.3	5.0	11.4	11.1
6. Grass	9.6	4.7	5.7	4.2	7.1	7.6
7. Crop	9.8	6.8	6.4	15.2	22.2	24.1
8. Barren	0	0	0	0.3	1.0	1.0
mean error	7.2	5.7	5.7	5.4	8.0	7.9

Table 5: Secular trends in ERA5-Land T_{2m}, Z_C, TRMM Precipitation, MODIS NDVI, MEaSUREs tree-cover fraction and surface area with positive or negative trends in MEaSUREs tree cover for 8 land-cover classes (columns 'TMCF' through 'Barren') as well as for locations of TMCFs identified by Aldrich et al. (1997) (column marked 'Sites'). Zero trends with significance of $p > 0.05$ are indicated by a '-'.

	Sites	TMCF	EBL	DBL	SAV	Shrub	Grass	Crop	Barren
ERA5 T_{2m} ($10 \times$ K y^{-1}): 1981–2019									
Tropics	0.20	0.20	0.32	0.26	0.29	0.20	0.26	0.21	0.39
Americas	0.24	0.23	0.34	0.34	0.34	0.21	0.25	0.34	0.17
Africa	0.20	0.19	0.38	0.27	0.27	0.21	0.29	0.30	0.40
Asia	0.15	0.15	0.20	0.18	0.16	0.19	-	0.13	-
ERA5 $T_{d,2m}$ ($10 \times$ K y^{-1}): 1981–2019									
Tropics	0.24	0.23	0.24	0.23	0.17	-	0.24	0.38	0.47
Americas	0.18	0.16	0.19	0.13	0.07	-	0.09	0.19	-
Africa	0.30	0.27	0.34	0.21	0.23	0.19	0.29	0.34	0.49
Asia	0.31	0.30	0.32	0.35	0.34	-	0.19	0.44	0.32
ERA5 Z_C (m y^{-1}): 1981–2019									
Tropics	-0.55	-0.39	0.97	0.5	1.46	-	-	-2.17	-
Americas	0.84	0.89	1.92	2.69	3.39	-	2.00	1.95	4.09
Africa	-1.26	-0.98	-	-	-	-	-	-	-
Asia	-2.08	-1.79	-1.48	-2.13	-2.32	-	-	-3.88	-
TRMM Precipitation (mm y^{-1}): 1998–2019									
Tropics	-	-	-	-	-	-8.82	-3.88	-	-
Americas	-	-8.57	-	-	-	-	-6.66	-	-
Africa	-	-	-8.02	-	-	-	-	-6.79	-
Asia	-	-	-	-	-	-14.83	-	-	-
MODIS NDVI $\times$ 1000 (- y^{-1}): 2000–2019									
Tropics	0.78	0.96	0.45	0.71	0.54	-	-	1.39	-
Americas	0.91	1.07	0.36	-	-	0.52	-	0.96	0.35

Table 6: Total area of land-cover classes estimated with the Random Forest Classifier (Section 3.1) and areal extent showing significant positive or negative secular trends in MEaSUREs tree cover (Song et al., 2018) for each of the 8 land-cover classes.

	TMCF	EBL	DBL	SAV	Shrub	Grass	Crop	Barren
Total Area (km^2 $\times$ 1000)								
Tropics	2120	10030	3930	10310	2780	10290	2630	7270
Americas	1010	6080	1090	4470	190	1590	370	260
Africa	310	1870	1790	4840	1090	6960	710	7000
Asia	790	2070	1050	1000	1510	1740	1550	10
Area with positive secular trend in tree cover (km^2 $\times$ 1000)								
Tropics	1590	5000	1890	4450	340	4560	1860	80
Americas	790	2630	440	1500	30	630	260	30
Africa	160	830	730	2290	190	3200	390	50
Asia	650	1530	710	660	120	730	1210	1
Area with negative secular trend in tree cover (km^2 $\times$ 1000)								
Tropics	520	5030	2040	5850	1620	4410	750	30
Americas	220	3450	640	2970	40	940	110	10
Africa	150	1040	1060	2560	440	2480	310	20
Asia	150	540	340	330	1140	990	320	0